Title: Mesoporous tin oxide: An efficient catalyst with versatile applications in acid and oxidation catalysis

Authors: Pandian Manjunathan, Vijaykumar S. Marakatti, Prakash Chandra, Atul B. Kulal, Shubhangi B. Umbarkar, Raman Ravishankar, Ganapati V. Shanbhag

PII: S0920-5861(17)30686-7
DOI: https://doi.org/10.1016/j.cattod.2017.10.009
Reference: CATTOD 11076

To appear in: *Catalysis Today*

Received date: 4-4-2017
Revised date: 21-9-2017
Accepted date: 4-10-2017

Please cite this article as: Pandian Manjunathan, Vijaykumar S.Marakatti, Prakash Chandra, Atul B.Kulal, Shubhangi B.Umbarkar, Raman Ravishankar, Ganapati V.Shanbhag, Mesoporous tin oxide: An efficient catalyst with versatile applications in acid and oxidation catalysis, Catalysis Today https://doi.org/10.1016/j.cattod.2017.10.009

Mesoporous tin oxide: An efficient catalyst with versatile applications in acid and oxidation catalysis

Pandian Manjunathan,[a,b] Vijaykumar S. Marakatti,[a] Prakash Chandra,[a] Atul B. Kulal,[c] Shubhangi B. Umbarkar,[c] Raman Ravishankar[d] and Ganapati V. Shanbhag*[a]

[a]*Materials Science Department, Poornaprajna Institute of Scientific Research (PPISR), Bidalur Post, Devanahalli, Bengaluru-562164, India*

[b]*Graduate Studies, Manipal University, Manipal-576104, Karnataka, India*

[c]*Catalysis Division, CSIR-National Chemical Laboratory, Dr Homi Bhabha Road, Pune - 411008, India*

[d]*Hindustan Petroleum Green Research & Development Centre, Hindustan Petroleum Corporation Ltd. (HPCL),KIADB Industrial Area, Tarabahalli, Hoskote Taluk, Bengaluru - 560067, Karnataka, India*

Corresponding author: shanbhag@poornaprajna.org, gvshanbhag@gmail.com

Graphical abstract

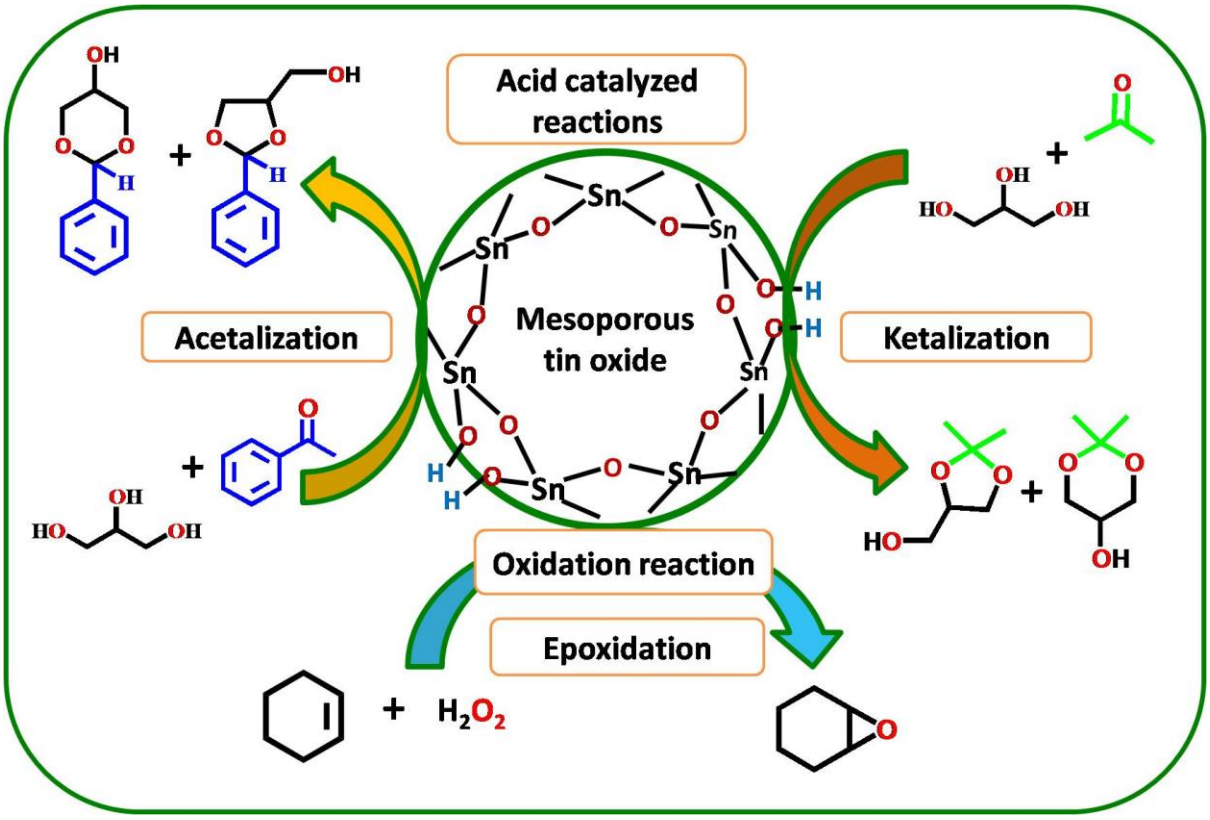

- Catalyst
- Acetalization
- Ketalization
- Epoxidation
- Glycerol

Highlights

- Nature, strength and amount of acidity in meso-SnO_2 were tuned by calcination
- Meso-SnO_2 showed high catalytic activity compared to other solid catalysts
- Brønsted acidic sites were found to be active sites for the studied reactions
- Direct correlation of amount of acidity with catalyst performance in meso-SnO_2

ABSTRACT

Mesoporous tin oxide was prepared by template assisted and template-free methods. As-prepared materials were calcined at various temperatures to generate different nature (Brønsted and Lewis), amount and strength of acidic sites. The physico-chemical properties of the catalysts were studied by XRD, N_2 sorption, pyridine-FTIR, NH_3-TPD, DRS UV-vis, TGA, SEM, TEM, ^{1}H MAS and ^{119}Sn MAS NMR analyses. The catalytic behavior of mesoporous

tin oxide catalysts was evaluated for acetalization and ketalization of glycerol with benzaldehyde and acetone respectively under solvent free conditions. The catalytic performance of mesoporous tin oxide was compared with that of other conventional solid acid catalysts namely H-ZSM-5, H-mordenite, H-beta, Al-MCM-41, Al-SBA-15 and Al-TUD-1. The efficiency of mesoporous tin oxide was also tested for cyclohexene epoxidation reaction. The catalyst prepared by template assisted method showed excellent catalytic performance compared to other catalysts due the difference in nature and amount of acidic sites in the catalyst. Meso-SnO_2-T-350 was stable and reusable catalyst for four cycles without any appreciable loss in activity, and therefore it offers a good catalyst for potentially wide applications.

Keywords: Mesoporous tin oxide

1. Introduction

Discoveries of ordered mesoporous silicas and other mesoporous supports like oxides, phosphates, carbons, polymers and organic–inorganic hybrid periodic mesoporous organosilicas through supramolecular templating pathways helped in developing high performance catalysts for the synthesis of fine chemicals [1–6]. Interest in employing wide range of mesoporous materials in catalysis has dramatically increased so far and their environmental aspects for clean chemical synthesis have been well established. Due to their interesting properties like high surface area, tunable pore size and their diverse frameworks, mesoporous materials have attracted immense interest in green catalytic processes. The presence of mesopores (pore size ranging from 2 – 50 nm) in catalysts can overcome diffusion constraints which are seen in microporous catalysts (pore size < 2nm), and the presence of large surface area facilitates ease accessibility of active sites to the reactant molecules leading to a better catalytic performance. In addition to their wide range of applications in organic and fine chemicals synthesis, mesoporous materials have also been used in adsorption, sensors, lithium-ion batteries, drug delivery, and nanodevices [7].

Metal oxides are found to be interesting materials owing to their acid–base and redox properties. The surface of metal oxides may terminate with M–OH, M–O–M, M=O or M– (O-vacant) functionalities [8]. Additionally, metal oxides possessing mesoporosity can be excellent catalysts since they endow properties of mesoporous materials and metal oxides. The nature of active sites in these metal oxides can be modulated by adopting different synthetic strategies and activation steps (calcination temperature). This leads to generation of active sites with a combination of Brønsted and Lewis characters which can be tuned by changing synthesis conditions.

Several tin based heterogeneous catalysts have contributed significantly in liquid phase organic transformations and biomass conversion. Tin containing zeolites have been used for

isomerisation of glucose [9], 1,3-dihydroxyacetone conversion into ethyl lactate [10], Sn-MFI as Lewis acid catalysts for isomerisation of cellulosic sugar [11], Sn-beta zeolite for the synthesis of 5-hydroxymethylfurfural from carbohydrates [12]. Zeolite Sn-MWW was used for the conversion of sugar into methyl lactate and lactic acid [13]. Sn-silicates were used for hydroxylation of phenol [14,15], whereas Sn-silicate with MFI structure was employed for ethylbenzene oxidation reaction [16]. Among other Sn based catalysts, Sn-MCM-41, Sn-SBA-15 and Sn(OH)Cl have been used for the synthesis of nopol [17–19]. Also, Sn(IV) grafted on MCM-41 gave good performance for Baeyer-Villiger oxidation reaction [20]. Hence, several tin based heterogeneous catalysts have been investigated and have proven to be promising candidates for different organic transformations. However, tin dioxide (SnO_2) has not been exploited much as a catalyst (not as mere support) in spite of having variable valence state and oxygen vacancy defects as its unique characteristics [21]. Recently, our group has reported the application of mesoporous SnO_2 as catalyst for few organic transformation reactions [22].

Glycerol is one of the most abundant platform chemicals obtained as a by-product during biodiesel synthesis. As surplus amount of glycerol is produced, it triggered the researchers to transform glycerol into value-added products *viz.*, chemicals and fuel additives. Glycerol can be transformed into various important products like acetins [23], acrolein [24], *tert*–butyl glycerol ethers [25], glycerol carbonate [26,27], 1,3-propanediol [28], 1,3-dihydroxyacetone [29], solketal [30] and more [31]. Glycerol undergoes acetalization (with aldehyde) and ketalization (with ketone) which results into the formation of isomeric six- and five-membered cyclic acetals respectively. The six-membered cyclic acetals are potential precursors to produce green platform chemicals 1,3-dihydroxyacetone and 1,3-propanediol [32]. The five-membered cyclic acetal (solketal) obtained from glycerol ketalization with acetone can be used as a cold flow improver to enhance cold weather performance of diesel fuel, which is also used as additive in ointments in the chemical industry [30,33].

Epoxidation of olefins is another class of reaction used for the synthesis of epoxide which acts as precursor for commodity chemicals such as drug intermediates, agrochemicals and food additives [34,35]. The choice of hydrogen peroxide as oxidant in olefin epoxidation reaction is advantageous from the view of environmental concern and green chemistry, since it generates water as the side-product. Moreover, it is cheaper and safer to use than organic peroxides or peracids [36].

Our earlier results inspired us to further explore the properties of mesoporous SnO_2 and its application as a catalyst in important organic transformations. In this study, we report mesoporous SnO_2 as an acid catalyst for the synthesis of 5-hydroxy-2-phenyl-1,3-dioxane and solketal from acetalization and ketalization of glycerol respectively, and cyclohexeneoxide from epoxidation of cyclohexene. The mesoporous SnO_2 was synthesized by supramolecular template and template-free approach and the active sites were modulated by varying calcination temperature. The catalytic performance of mesoporous SnO_2 was evaluated by comparing with other well-known mesoporous (Al-MCM-41, Al-SBA-15 and Al-TUD-1) and microporous (H-ZSM-5, H-mordenite and H-beta zeolite) catalysts. A clear correlation of B/L ratio and acidic sites with catalytic performance was obtained.

2. Experimental

2.1. Chemicals and Materials

Cetyltrimethylammonium bromide (CTAB) and tin chloride pentahydrate were purchased from Loba Chemie Pvt. Ltd, India. Ammonium hydroxide (25 wt%), acetone, benzaldehyde, cyclohexene, glycerol, hydrogen peroxide (50%) and methanol were purchased from Merck India Pvt. Ltd. Tetraethyl orthosilicate, tetraethyleneglycol, cyclohexeneoxide and solketal were purchased from Sigma Aldrich Pvt. Ltd, India. NH_4-Beta zeolite (SAR = 25) was obtained from Nankai, China. NH_4-ZSM-5 zeolite (SAR = 30) was purchased from Zeolyst

International. H-Mordenite zeolite (SAR = 16) was kindly donated by Sud-Chemie India Pvt. Ltd, India.

2.2. Catalyst preparation

Synthesis of mesoporous tin oxide by template assisted and template-free method

The mesoporous tin oxide was synthesized at room temperature using $SnCl_4 \cdot 5H_2O$ as the tin precursor and cetyltrimethylammonium bromide (CTAB) as the template [22,37,38]. In a typical procedure, 18 g of CTAB was dissolved in 150 ml of distilled water under stirring to get a homogeneous solution. To this solution, 12 ml of NH_4OH (25 wt%) dissolved in 48 ml of distilled H_2O was added under stirring. Further, aq. $SnCl_4$ (15 g of $SnCl_4 \cdot 5H_2O$ dissolved in 150 ml distilled water) was added drop wise to this solution under continuous stirring to obtain a white slurry. It was stirred for 3 h followed by aging at room temperature for 48 h. The obtained product was filtered, washed with distilled water and dried at 120 °C. The as-prepared white solid was calcined at different temperatures of 300, 350, 400 and 500 °C under the flow of air with a heating rate of 2 °C min^{-1} for 2 h. The obtained yellow solid samples are designated as meso-SnO_2-T-*x* (where T = template assisted synthesis, x = calcination temperature).

The template-free synthesis of tin oxide was carried out by adopting the aforementioned procedure in the absence of CTAB. The obtained product was filtered, washed, dried and calcined at respective temperatures and are designated as meso-SnO_2-TF-*x*. Other mesoporous catalysts namely Al-MCM-41 (SAR = 25), Al-SBA-15 (SAR = 30) and Al-TUD-1 (SAR = 30) were prepared from the reported literature [39–41]. The ammonium forms of zeolites were calcined at 540 °C under static air for 4 h with the ramp rate of 5 °C min^{-1} to convert ammonium form into protonic form. The obtained samples were labelled as H-beta, H-ZSM-5 and H-mordenite.

2.3. Catalyst characterization

The powder X-ray diffraction of the catalysts was recorded with Bruker D2 phaser X-ray diffractometer using CuKα radiation (λ =1.5418 Å) with high resolution Lynxeye detector. The mean crystallite sizes of the samples were calculated according to the Scherrer equation using the full width at half maximum intensity (FWHM) of the (110) plane.

Scherrer equation, $D_p = \frac{k\lambda}{\beta\cos\theta}$

D_p is the mean crystallite size, k= 0.94, λ= X-ray wavelength; β is the full width at half maximum intensity (FWHM) of the (110) plane, θ is the Bragg angle (in degrees).

Nitrogen sorption measurements of catalysts were performed at 77 K using Quantachrome instrument. The specific surface areas of the samples were calculated by using the Brunauer–Emmett–Teller (BET) method in relative pressure (P/P_0) range of 0.05 to 0.25. The pore-size distributions of the samples were determined by Barrett–Joyner–Halenda (BJH) method. The total pore volume of each catalyst was accumulated at a relative pressure of P/P_0=0.99.

The Brønsted and Lewis acidic sites in catalysts were investigated by pyridine adsorption study using FT-IR (Bruker α-T model). The self supported wafers of the catalysts were prepared by a pellet press instrument. The wafer was then calcined at the respective calcination temperatures of the catalysts for 1 h, later cooled to 250 °C and placed in a desiccator to maintain moisture free condition. Then the samples were saturated with pyridine and heated at 150 °C for 1 h to remove physisorbed pyridine. FTIR spectra were recorded in absorbance mode in the wavelength range from 1400 to 1600 cm^{-1}. The spectrum obtained after pyridine treatment was subtracted with spectrum of pyridine untreated sample to get peaks only due to pyridine–acid interaction. The B/L ratio was calculated from the relative peak intensity obtained at the frequency 1545 and 1450 cm^{-1} [30].

The amount of acidity present in the catalysts were determined by temperature programmed desorption instrument equipped with thermal conductivity detector using ammonia as a probe molecule. In all the experiments, the sample (200 mg) was calcined at the desired temperature for 1 h in helium gas flow (25 mL min^{-1}) and then cooled to 50 °C. At 50 °C, the sample was saturated with 10% of ammonia in a helium stream for 30 min. After the saturation of probe molecule, the sample was flushed with helium for 1 h at 50 °C to remove the physisorbed probe molecule, and then desorption of ammonia was performed in the temperature range from 50 to 600 °C (till its calcination temperature) with a heating rate of 8 °C min^{-1}[30].

The UV–vis DRS spectra of tin oxide samples were recorded on a Perkin Elmer Lambda 650 UV/Vis spectrometer equipped with an integration sphere diffused reflectance attachment. The spectra were obtained in the range of 200 – 800 nm against the $BaSO_4$ as reference.

The ^{1}H and ^{119}Sn MAS NMR spectra of the samples were recorded on Bruker instrument. The resonance frequencies for ^{1}H and ^{119}Sn were 399.78 and 149.08 MHz respectively. ^{1}H MAS NMR analysis was performed with the operation condition at spinning rate of 8KHz with 5 s relaxation delay for 200 scans. ^{119}Sn MAS NMR analysis was performed with the condition of spinning rate of 8KHz with 10 s relaxation delay for 6000 scans. The chemical shifts were referenced to tetramethylsilane (TMS) for ^{1}H and tin oxide for ^{119}Sn respectively [42].

TGA curves were recorded using a Universal V 2.4F-TA analyzer by heating the sample from room temperature to 800 °C at the rate of 10 °C min^{-1} in flowing of nitrogen gas.

Scanning electron microscopy (SEM) images of tin oxide catalysts were recorded in Zeiss microscope to investigate the particle size and morphology. The transmission electron microscopy (TEM) images, selected-area electron diffraction (SAED) patterns, and high-

resolution transmission electron microscope (HRTEM) images were recorded on a TEM-JEOL-2010 instrument.

2.4. Catalytic activity studies

General procedure for catalytic experiments

The glycerol acetalization reaction with benzaldehyde was performed in a 50 mL 2-necked glass batch reactor equipped with a reflux condenser. In a typical experiment, the required amounts of glycerol and benzaldehyde were taken along with preactivated catalyst (wt% referred to glycerol weight). The reaction mixture was flushed with nitrogen gas in order to remove air to avoid aerobic oxidation of benzaldehyde. Then, reaction mixture was magnetically stirred at required temperature under nitrogen atmosphere.

The glycerol ketalization reaction with acetone was performed in a 25 mL glass batch reactor equipped with a reflux condenser. In a typical experiment, the required amounts of glycerol and acetone were taken along with preactivated catalyst (wt% referred to glycerol weight) and reaction mixture was magnetically stirred at required temperature.

Cyclohexene epoxidation was performed using a 25 mL glass batch reactor equipped with a reflux condenser. In a typical experiment, 10 mmol cyclohexene, 40 mmol H_2O_2 and 8 mL acetonitrile (as solvent) were taken along with 10 wt% (referred to weight of cyclohexene) of pretreated catalyst, and magentically stirred at 80 °C.

Analysis procedure for glycerol reactions: After the desired time, the reaction mixture was taken in methanol and centrifuged to separate out the catalyst from liquid phase. The obtained liquid was analyzed by gas chromatography (Agilent 7820A) equipped with a capillary column (0.25 mm I.D and 60 m length, HP-INNOWAX) and flame ionization detector. The glycerol conversion and product yield were calculated using the following formulae:

$$\text{Glycerol conversion (mol\%)} = \frac{(\text{moles of glycerol taken} - \text{moles of unreacted glycerol})}{\text{moles of glycerol taken}} \text{ X } 100$$

$$\text{Product yield (mol\%)} = \frac{\text{moles of glycerol converted (\%) X desired product selectivity (\%)}}{100\ (\%)}$$

Analysis procedure for cyclohexene epoxidation reaction: After a desired time, the reaction mixture was centrifuged in order to separate out the catalyst from the liquid phase. The obtained liquid was analyzed by gas chromatography (Agilent 7820A) equipped with a capillary column (0.25 mm I.D and 30 m length, HP-5) and flame ionization detector. The cyclohexene conversion and product selectivity were calculated using the following formulae:

$$\text{Cyclohexene conversion (mol\%)} = \frac{(\text{moles of cyclohexene taken} - \text{moles of unreacted cyclohexene})}{\text{moles of cyclohexene taken}} \text{ X } 100$$

$$\text{Product selectivity (mol\%)} = \frac{\text{moles of desired product}}{\text{moles of cyclohexene converted}} \text{ X } 100$$

3. Results and discussion

3.1 Characterization

X-ray diffraction: The low angle XRD patterns of the meso-SnO_2-T (template assisted mesoporous tin oxide) calcined at different temperatures are shown in Fig. 1a. The mesoporous tin oxide calcined at 300 °C (meso-SnO_2-T-300) shows the presence of diffraction peak which can be indexed as (100) reflection due to two-dimensional hexagonal structure. However, calcination of mesoporous tin oxide at ≥ 350 °C resulted in the disappearance of low angle diffraction peak which is attributed to the loss of orderedness in the mesoporous structure due to sintering at high temperatures [43–45].

The wide angle XRD patterns of calcined tin oxide catalysts are depicted in Fig. 1b and it shows diffraction peaks which can be indexed to (110), (101), (200) and (211) reflections assigned to a tetragonal rutile crystal structure with space group of P42/mnm. XRD patterns of tin oxide showed narrowing of diffraction peaks by increasing the calcination temperatures from 300 – 500 °C, suggesting the gradual increase of crystallinity due to the agglomeration of crystallites. The crystallite size of tin oxide determined by Scherrer equation confirms the increase of crystallite size from 4.4 to 13.8 nm with increase in calcination temperatures in the range of 300−500 °C (Table S1). Interestingly, template-free tin oxide (meso-SnO_2-TF-350) showed a similar crystallite size compared to template assisted tin oxide (meso-SnO_2-T-350).

Nitrogen sorption: The textural properties of the catalysts were investigated by N_2 sorption measurements and tabulated in Table 1. Fig. 2 (a and b) shows the adsorption and desorption curves of nitrogen which makes it evident that tin oxide has a typical type IV isotherm which is characteristic of mesoporous materials. The meso-SnO_2-T-300 and meso-SnO_2-T-350 show H2-type hysteresis loop, indicative of cavitation effect in ink bottle type pores which could be attributed to the formation of spherical pores along with the cylindrical pores present in the materials. However, meso-SnO_2-T-400 and meso-SnO_2-T-500 possess H1-type hysteresis

suggesting a well-defined cylindrical-like pore channels present in the porous system [46–48]. Apparently, the pore diameter of tin oxide increased systematically from 3.4 to 6.7 nm with an increase in calcination temperatures confirming the presence of mesoporosity. The surface area, pore volume and pore size of tin oxide and other catalysts are given in Table 1. The meso-SnO_2-T-300 exhibited a highest surface area of 160 m^2g^{-1} among all the tin oxide samples. However, further increase of calcination temperature > 300 °C results in significant decrease of surface area from 160 to 51 m^2g^{-1}. The decrease in surface area and pore volume of tin oxide could be ascribed to the sintering and destruction of pores at higher calcination temperatures [22,37,38]. Interestingly, the template-free meso-SnO_2-TF-350 showed a type IV isotherm with a H2-type hysteresis loop and the presence of mesoporosity with the pore size of 5.3 nm. Although the meso-SnO_2-TF-350 exhibited mesoporsity, it showed lower surface area and pore volume compared to meso-SnO_2-T-350 which suggests the role of template during the synthesis.

Pyridine-FTIR: Pyridine-FTIR studies were performed to distinguish the nature of acidic sites in the catalysts (Fig. S1). The relative ratios of Brønsted to Lewis acidic sites of catalysts were calculated from the intensity of PyH^+ and PyL peaks (1545 and 1450 cm^{-1} respectively). These peaks arise due to the interaction of pyridine with Brønsted and Lewis acid sites present on the catalyst surface and are listed in Table 1. The meso-SnO_2-T exhibits both Brønsted and Lewis acidic sites with a systematic decline in B/L ratio with increase in the calcination temperature due to dehydroxylation at higher temperatures. The presence of Brønsted acidity in the catalyst could be attributed to the surface Sn–OH or hydrogen bonded Sn–OH groups, whereas Lewis acidity arises due to the framework Sn^{4+} sites [22]. The py-FTIR of other catalysts namely Al-MCM-41, Al-SBA-15, Al-TUD-1, H-beta, H-ZSM-5 and H-mordenite also showed a combination of Brønsted and Lewis acidity with varying B/L values.

NH_3-TPD: The amounts of acidity in mesoporous tin oxide catalysts were determined by temperature programmed desorption using ammonia as a probe molecule (NH_3-TPD) (Fig. 3 and Table 1). The NH_3–TPD measurements of mesoporous tin oxide were carried out up to its calcination temperature since the material undergoes dehydroxylation beyond its calcination temperature. The total amount of acidic sites in the meso-SnO_2-T catalyst reduced significantly with increasing of calcination temperatures > 350 °C. The decrease in total acidity could be attributed to the decrease of surface area and dehydroxylation of surface active sites at higher temperatures. Meso-SnO_2-TF-350 (template-free tin oxide) catalyst showed a lower amount of acidity than meso-SnO_2-T-350 (template assisted) which could be due to its lower surface area. In general, mesoporous SnO_2 samples contained a lower amount of acidic sites compared to Al-MCM-41, Al-SBA-15, Al-TUD-1, H-beta, H-ZSM-5 and H-mordenite catalysts (Table 1).

UV-vis DRS*:* The UV-vis DRS studies were performed for template-free (meso-SnO_2-TF) and template assisted tin oxide (meso-SnO_2-T) and depicted in Fig. 4. The spectra of the sample showed three absorption bands in the range of 200 – 400 nm suggesting the presence of Sn in different coordination environment. The absorbance around 207 nm corresponded to the tetrahedrally coordinated Sn^{4+}, which often assumed to be Lewis acidic sites, while the absorbance band around 224 nm was attributed to the Sn^{4+} in octahedral coordination which was assumed to be Brønsted acidic sites. Additionally, the absorbance around 280 nm was due to a hexa co-ordinated polymeric Sn–O–Sn type species in SnO_2. Notably, the absence of band around 280 nm in the uncalcined sample (meso-SnO_2-TF-120) suggested that the formation of Sn–O–Sn species in calcined samples was due to the polymerization of Sn species [49–51].

^{1}H MAS NMR*:* It is an important technique which gives information about the relative strength of acidic sites in the material from the change in chemical shift due to bond polarization. As the calcination temperature of meso-SnO_2-T increased from 300 to 350 °C, the chemical shift showed an increment from 6.43 to 6.63 ppm (Fig. 5a). The low-field shift indicated an increase

in acidic strength of the catalyst. The change in the chemical shift of ^{1}H could be caused by weak hydrogen bonding in SnO–H. Higher the chemical shift towards low-field, greater is the strength of acidic sites due to a greater extent of bond polarization of SnO–H. Weaker bond strength of SnO–H corresponds to higher "intrinsic" acidic strength [42,19]. The chemical shift of meso-SnO_2-T calcined above 350 °C shifts towards high-field from 6.63 to 6.51 ppm indicating that strength of acidic sites slightly decreases upon increasing of calcination temperature above 350 °C. The chemical shift of meso-SnO_2-T-350 at low-field was attributed to the presence of relatively stronger acidic sites compared with other meso-SnO_2-T catalysts. ^{1}H MAS NMR spectra of meso-SnO_2-T and meso-SnO_2-TF are shown in Fig. 5b. Both the samples exhibit peaks at identical chemical shift of 6.63 ppm which indicates the presence of similar strength of acidic sites in them.

^{119}Sn MAS NMR: The UV−Vis DRS analysis results revealed that Sn species in meso SnO_2 samples were coordinated in tetrahedral and octahedral environment leading to a further study in this regard. ^{119}Sn MAS NMR spectroscopy provides the coordination states of Sn species and the results are shown in Fig. 5c. Meso-SnO_2-T-350 and meso-SnO_2-TF-350 gave NMR peaks at -491 ppm, -547 ppm, -604 ppm, -656 ppm and -711 ppm. In the literature, the main resonance signal at −604 ppm is reported to be characteristic of octahedrally co-ordinated Sn species [52]. These results suggest that the SnO_2 prepared by template and template-free routes possessed Sn species in similar coordination environment.

Scanning electron microscopic analysis: The morphology and particle size of meso-SnO_2 calcined at different temperatures were determined by SEM analysis and the images are shown in Fig 6. All the meso-SnO_2-T calcined at different temperatures possessed non-uniform particles with rough-edged morphology of varying average particle size from 3.1 – 5.8 μm. Meso-SnO_2-T catalysts calcined at 300 and 350 °C showed similar particle size of 3.1μm. Further increase in calcination temperature from 350 to 500 increased particle size from 3.1 to

5.8 μm which could be due to agglomeration of particles caused by sintering of particles at elevated temperatures. Meso-SnO_2-TF-350 (template-free) shows irregular morphology with average particle size of 1.6 μm which is smaller compared to meso-SnO_2-T-350 catalyst. The larger particle size in Meso-SnO_2-T-350 could be attributed to the influence of structure directing agent during the synthesis which results in the growth of particle size.

Transmission electron microscopic analysis: TEM, HRTEM, fast Fourier transform (FFT) pattern and SAED images of the meso-SnO_2-T-350 are shown in the Fig.7 (a–d). The TEM image of meso-SnO_2-T-350 demonstrates that the mesostructured SnO_2 is composed of nanocrystalline domains and it agrees with the results obtained from Scherrer calculation. TEM images also clearly confirmed the presence of disordered mesoporosity in meso-SnO_2-T-350. The SAED pattern exhibited the concentric rings indicating the presence of small crystallites with well-defined (110), (101), (200), (211) and (301) lattice planes. The HRTEM of meso-SnO_2-T-350 reveals well-defined lattice fringes corresponding to tetragonal rutile phase of SnO_2 with d-spacings of 0.33 and 0.26 nm for (110) and (101) planes respectively. The FFT pattern of the meso-SnO_2-T-350 further confirms low crystallinity of the sample and diffraction spots could be indexed to tetragonal SnO_2 corresponding to (110) and (101) planes [44, 53, 54].

Thermogravimetric analysis: The TGA profile of tin oxide catalysts exhibited a weight loss in three steps (Fig. S2). As-synthesized meso-SnO_2-T-120 catalyst showed an initial weight loss of 5.6% below 120 °C due to a loss of water molecules. The second weight loss in the region of 120 – 400 °C was ascribed to the removal of the surfactant. The final small weight loss above 400 °C could be due to dehydroxylation. The meso-SnO_2 catalyst calcined at different temperatures showed a negligible weight loss as compared to as-synthesized catalyst indicating a complete removal of the surfactant, and the weight loss was attributed to the dehydroxylation of hydroxyl group in Sn–OH to form Sn–O–Sn [22].

3.2. Catalytic activity studies

The catalytic behavior of mesoporous tin oxide was evaluated by performing three reactions, namely acetalization of glycerol with benzaldehyde, ketalization of glycerol with acetone and oxidation of cyclohexene in the presence of hydrogen peroxide.

3.2.1. Acetalization of glycerol with benzaldehyde

Glycerol acetalization with aldehydes results into the formation of isomeric five- and six-membered cyclic acetals (Scheme 1). The six-membered cyclic acetal [5-hyroxy-2-phenyl-1,3-dioxane (HPD)] is a potential precursor to produce green platform chemicals *viz.*, 1,3-dihydroxyacetone and 1,3-propanediol *via* hydrogenation and oxidation processes respectively [32]. Direct synthesis of 1,3-propanediol by glycerol hydrogenolysis reaction is limited to lab scale due to a high temperature and pressure conditions. However, 1,3-propanediol can be selectively produced from glycerol by a new approach described by Wang et al involving selective transformation of secondary hydroxyl group of glycerol into a tosyloxy group and then removing the transformed group by catalytic hydrogenolysis [55,56].

A variety of solid acid catalysts have been investigated for acetalization of glycerol with benzaldehyde. MoO_3/SiO_2 [57], ZrO_2, TiO_2–ZrO_2, MoO_x/ZrO_2, and MoO_x/TiO_2–ZrO_2 [58] amberlyst-36, H-beta, nafion and montmorillonite K-10 [59] catalysts were studied for this reaction in presence of a solvent. The use of solvent in the reaction medium has certain practical difficulties in the purification of products. In order to overcome these problems, reactions under solvent free conditions are most desirable. Catalysts *viz*. SO_4^{2-}/SnO_2, MoO_3/SnO_2, WO_3/SnO_2 [60], SiW/MCM-41 [61], Al-SBA-15 [62], Fe/Al-SBA-15 [63] are reported under solvent free conditions. H-beta and amberlyst-36 are reported to be best catalysts in the literature. They gave around 94% conversion with 60% selectivity to HPD.

3.2.1.1. Catalyst screening studies

The catalytic behavior of meso-SnO_2-T-*x* as well as conventional microporous and mesoporous catalysts were evaluated for glycerol acetalization with benzaldehyde under solvent free condition (Table 2).

Prior to catalytic reaction, a blank run without catalyst was performed. The reaction without a catalyst resulted in only 21% of glycerol conversion with ~46% HPD selectivity. Among the catalysts screened in this study, mesoporous tin oxide (meso-SnO_2-T-350) exhibited a greater catalytic performance even though it contains lower amount of acidic sites compared to microporous and mesoporous catalysts. The greater catalytic activity of meso-SnO_2-T-350 can be attributed to the presence of higher B/L ratio (3.2), since the reaction is predominately catalyzed by Brønsted acidic sites. The catalytic activity of meso-SnO_2-TF-350 (template-free tin oxide) was lower than meso-SnO_2-T-350 which could be attributed to the presence of lower amount of acidity and surface area. Among the zeolites, with glycerol conversion of 60.4%, H-beta exhibited a higher catalytic activity than H-mordenite and H-ZSM-5. The higher performance of H-beta zeolite could be attributed to the presence of large pore size. Mesoporous solid acid catalysts *viz.* Al-MCM-41, Al-SBA-15 and Al-TUD-1 were also investigated to study the behaviour of porosity towards the reaction. Mesoporous acid catalysts showed lower glycerol conversion of < 50% with similar (~ 48%) HPD selectivity as observed for H-beta zeolite. The lower conversion using mesoporous catalysts could be due to lower amount of acidic sites in the catalysts. In order to measure the efficiency of catalysts, the turn over frequency (TOF) was calculated. Mesoporous catalysts showed higher TOF compared to microporous zeolites which suggests the role of mesoporosity towards the reaction. The TOF of catalysts decreased in the following trend (refer Table 2): Meso-SnO_2-T-350 > Al-SBA-15 > Al-MCM-41 > Al-TUD-1 > H-beta (large pore) > H-ZSM-5 (medium pore) > H-mordenite (1D dual pore). It should be noted that the TOF of H-beta zeolite was 3 times lower than meso-SnO_2-T-350. Further, H-beta zeolite with identical amount of acidic

sites as in meso-SnO_2-T-350 was taken in the reaction. It showed 42.1% glycerol conversion with 47% HPD selectivity lower than meso-SnO_2-T-350. The greater catalytic performance of meso-SnO_2-T-350 could be attributed to a combination of mesoporosity and the nature of acidic sites which offers better distribution of active sites leading to easy accessibility to the reactant molecules and facilitates easy diffusivity of molecules over microporous catalysts. It is evident from the study that the mesoporous tin oxide exhibited superior performance over microporous and mesoporous catalysts even though it contains lower amount of acidic sites. These results show that the performance of catalysts mainly depends upon the amount and nature of acidic sites.

3.2.1.2. Catalytic behavior of meso-SnO_2-T-x calcined at different temperatures:

A series of meso-SnO_2-T-*x* catalyst calcined at temperatures ranging from 300 to 500 °C bearing different amount of acidic sites were used to study the effect of acidity towards the glycerol acetalization with benzaldehye (Fig. 8). The glycerol conversion increased appreciably from 57.3 to 60.2% upon increasing the calcination temperature of meso-SnO_2-T-*x* from 300 to 350 °C. However, further increasing of calcination temperature from 350 to 500 °C resulted in decrease of the conversion considerably (from 60.2 to 51.8%) with similar HPD selectivity (~50%).

In order to understand the catalytic behavior of the catalysts calcined at different temperatures, the physico-chemical properties and their relationship with catalytic performance were studied (Table 1). It is observed that the total amount of acidic sites and B/L ratio decreased with increase in calcination temperatures from 350 to 500 °C. The decrease in active sites upon increasing calcination temperature could be attributed to the decrease of surface area and increase in particle size due to agglomeration of particles resulting in less surface metal-oxygen pairs which is also evident from nitrogen sorption studies [64,26]. Relationship between the amount of acidic sites in meso-SnO_2-T-*x* catalysts and their catalytic activity on

glycerol conversion is depicted in Fig. 8. The enhanced catalytic perfromance of meso-SnO_2-T-350 was mainly attributed to the presence of greater amount of acidic sites compared to other catalysts. Therefore, meso-SnO_2-T-350 catalyst was selected as the best catalyst for further studies.

3.2.1.3. Influence of reaction conditions

The effect of reaction temperature, reactant mole ratio and catalyst amount on the catalytic activity was studied.

The influence of reaction temperature was studied using meso-SnO_2-T-350 catalyst from 80 to 110 °C with glycerol: benzaldehyde mole ratio of 1:1 using 0.1 g of catalyst (10 wt% referred to glycerol mass) under N_2 atmosphere. The glycerol conversion found to increase marginally (49.5 to 60.2%) with increase in reaction temperature from 80 to 100 °C and the results are shown in Fig. 9a. However, the glycerol conversion remains almost the same with further increase of reaction temperature to 110 °C. Glycerol being more polar compared to benzaldehyde, it preferentially adsorbs onto the active sites. Therefore, higher concentration of carbonyl compound could be necessary to achieve greater conversion. There is no considerable change in HPD selectivity with increase in reaction temperature. Hence, the reaction temperature of 100 °C was selected for further studies.

The effect of mole ratio of benzaldehyde to glycerol on catalytic activity was studied at 100 °C using 10 wt% of meso-SnO_2-T-350 catalyst (wrt glycerol weight) under N_2 atmosphere. The mole ratio of benzaldehyde to glycerol was varied from 1 to 2.25 as shown in Fig. 9b. The glycerol conversion increased from 60.2 to 92.3% with increase in mole ratio from 1 to 2 due to an increase in availability of benzaldehyde to glycerol. It is observed that there is no improvement in glycerol conversion with further increase in mole ratio to 2.25, whereas selectivity to HPD decreased marginally from 50 to 48%. Initially the reaction proceeds at higher rate due to higher concentration of reactants in the medium. Once the product

concentration increases in the reaction medium, the concentration of the reactants decreases leading to a less accessibility to the active sites. Therefore, there might be higher adsorption of product molecules on the active sites resulting in not much improvement in the activity once the conversion reached > 90%. Based on the above results, benzaldehyde to glycerol mole ratio of 2 was found to be optimum condition for the catalytic transformation of glycerol to HPD.

The effect of catalyst amount for glycerol acetalization with benzaldehyde was studied at 100 °C with glycerol: benzaldehyde mole ratio of 1:2 under N_2 atmosphere using meso-SnO_2-T-350 catalyst (5 to 20 wt%) as shown in Fig. 9c. With the increase of catalyst amount from 5 to 10 wt%, the glycerol conversion significantly increased from 78.1 to 92.3% due to an increase in the number of accessible active sites to the reactant molecules. Further increasing the catalyst amount > 10wt% showed no significant improvement in the conversion and selectivity to HPD remained constant (48%). Hence, 10 wt% of catalyst with respect to glycerol was taken as an optimum catalyst weight required for this reaction.

The influence of reaction time for the synthesis of HPD was studied under optimized reaction conditions. The glycerol conversion and selectivity for HPD increased with increase of reaction time as shown in Fig. 9d. The glycerol conversion was 71.2% after 5 min and then reached to 92.3% after 30 min of reaction time. It shows that glycerol conversion marginally increased to 93.6 at higher reaction time at 120 min with almost similar selectivity to HPD. Initially, kinetically favoured product, 5-membered cyclic acetal forms at a higher rate than the 6-membered HPD (thermodynamically favoured product) [59]. However, with the progress of reaction, glycerol conversion increases with increase in selectivity for HPD due to the increase in thermodynamically favoured product to reach equilibrium between the two products. This increases the selectivity of 6-membered acetal with increase in reaction time.

3.2.2. Ketalization of glycerol with acetone:

Glycerol undergoes ketalization with acetone to produce solketal (5- membered) and 6-membered compounds (Scheme 2). Solketal can be used as a cold flow improver to enhance cold weather performance of diesel fuel and also reduces its viscosity. Solketal blended with regular gasoline in 1, 3 or 5 vol% decreases the gum formation and also it enhances the octane number up to 2.5 points [65–67]. It is used in cosmetics industry as an additive in ointments in the chemical industry and as an additive in low temperature transfer fluids [33]. A variety of acid catalysts namely $SnCl_2$ [68], SnF_2 [69], heteropoly acids [70], $Cs_{2.5}H_{0.5}PW_{12}O_{40}$ [30], heteropoly acids immobilized over silica [71], $(C_3H_7)_4N^+$/PWA [33], MoO_3/SiO_2 [30], MoO_3/SnO_2, WO_3/SnO_2, SO_4^{2-}/SnO_2 [48], SO_4^{2-}/ZrO_2 [72], TiO_2-SiO_2 [73], titanate nanotubes [74], Nb_2O_5 [75], niobium aluminium mixed oxides [76], niobium oxyhydroxide [77], nanoporous hydroxyapatite [78], Brønsted acid ionic liquids (BAILs) [79], sulfonated hollow sphere carbon [80], sulfonic acid-functionalized mesoporous polymer (MP-SO_3H) [81], acid functionalized carbon–silica-meso composite [82], acid functionalized activated carbons [83], montmorillonite K-10, amberlyst-15, zeolites [30,84], Ar-SBA-15 [85], aluminium triflate grafted MCM-41 [86], Sn-SBA-15 (S-Sn-OH) [87], Sn-TUD-1 [88], Fe/Al-SBA-15 [63], molybdenum phosphate supported on SBA-15 [89], MOF [90] have been employed for condensation reaction of glycerol and acetone.

3.2.2.1. Catalytic activity studies:

The catalytic efficiency of meso-SnO_2-T-350 in the synthesis of solketal *via* ketalization of glycerol with acetone was studied. The activity of the screened catalysts on its performance after 30 min reaction time was compared with other catalysts (Table 3). Prior to catalytic activity studies, blank run was carried out without a catalyst, which resulted in negligible glycerol conversion (0.1%) signifying that the reaction is truly catalytic. Mesoporous catalysts namely Al-MCM-41, Al-SBA-15 and Al-TUD-1 gave 35.5, 26.1 and 10.2% with the solketal selectivity of 94.2, 96.3 and 89.0% respectively. The greater activity

of Al-MCM-41 (TOF =154) compared to Al-TUD-1 (TOF = 45) could be attributed to its 2-dimensional ordered pore structure. Microporous catalysts, namely H-ZSM-5, H-mordenite and H-beta resulted in glycerol conversion of 34.1, 16.2 and 47.4% respectively. The higher activity of H-beta could be attributed to easy diffusivity of molecules in its large pores. The meso-SnO_2-T-350 showed higher glycerol conversion of 51.3% with 98.0% solketal selectivity compared to other catalysts investigated in this study. Higher activity of meso-SnO_2-T-350 could be attributed to the presence of mesoporosity and high B/L ratio of 3.2 since this reaction is predominantly catalyzed by Brønsted acidity. Meso-SnO_2-T-350 (template assisted) catalyst showed significantly greater glycerol conversion than meso-SnO_2-TF-350 (template-free) owing to the presence of higher amount of acidity and larger surface area. H-Beta zeolite with identical amount of acidic sites as in meso-SnO_2-T-350 was taken and performed the reaction. It showed 38.8% glycerol conversion with 97.6% selectivity to solketal. Overall, meso-SnO_2-T-350 exhibited a higher turnover frequency compared to other catalysts which signifies the importance of B/L ratio and mesoporosity towards the reaction. Thus, meso-SnO_2-T-350 is an efficient acid catalyst for the synthesis of solketal better than other conventional solid acid catalysts tested in this study.

3.2.2.2. Catalytic behavior of meso-SnO_2-T-x calcined at different temperatures:

Meso-SnO_2-T-x catalysts calcined at different temperatures ranging from 300 to 500 °C were investigated for the synthesis of solketal using the reaction conditions. A clear correlation was obtained for glycerol conversion with amount of acidic sites as presented in Fig. 10. Meso-SnO_2-T calcined at 300 °C gave 47.6% glycerol conversion with 97.5% solketal selectivity and further increase in calcination temperature of meso-SnO_2-T to 350 °C increased the conversion to 51.3%. The enhanced catalytic performance is attributed to increase in the presence of total acidity in meso-SnO_2-T-350. However, further increase of calcination tempearture ≥ 400 °C resulted in decline in glycerol conversion (48.7 to 42.4%) due to a

decrease in total acidity and increase in particle size. The superior catalytic behavior of meso-SnO_2-T-350 was due to the presence of higher amount of acidity than other meso-SnO_2 catalysts.

3.2.2.3. Influence of reaction conditions

The influence of reaction parameters *viz*. reaction temperature, reactants mole ratio and catalyst amount on the catalytic activity using meso-SnO_2-T-350 catalyst was investigated for glycerol acetalization with acetone.

The effect of reaction temperature was studied at different temperatures ranging from 30 to 70 °C using glycerol to acetone mole ratio of 1:1 for 30 min. The glycerol conversion and solketal selectivity was found to be low at 30 °C (Fig. 11a). The glycerol conversion increased significantly (from 33.5 to 51.3%) with increase in reaction temperature from 30 to 60 °C which also resulted in increase of solketal selectivity from 96 to 98.5%. Further increase of reaction temperature to 70 °C (reflux condition) resulted in 45.4% glycerol conversion which is marginally lower compared to 60 °C. Thus, 60 °C reaction temperature was found to be optimum for solketal synthesis, and hence it was taken for further studies.

The effect of different concentrations of reactants was studied with acetone to glycerol mole ratios varying from 1 to 6 at 60 °C using 5 wt% catalyst. Glycerol conversion increased significantly from 51.3 to 90.1% with increase in the mole ratio from 1 to 5 which could be due to increase in availability of acetone for the reaction (Fig. 11b). Nonetheless, further increase of mole ratio to 6 resulted in similar glycerol conversion and selectivity to solketal. Hence, acetone to glycerol mole ratio of 5 was used for further studies.

The influence of catalyst amount was studied by increasing the amount of catalyst from 1 to 7wt% and shown in Fig. 11c. As a result, with increase of the catalyst amount from 1 to 5 wt%, the glycerol conversion and solketal selectivity increased marginally from 78.7 to 90.1% and 95 to 98.5% respectively. This increase in activity was attributed to the increase of the

number of available acidic sites to the reactant molecules. Further addition of catalyst amount to 7wt% resulted in marginal decline in activity. Hence, 5wt% of catalyst was found to be optimum and used for further studies.

The effect of reaction time on solketal synthesis was studied under the optimized reaction conditions (Fig. 11d). Initially it gave 73% conversion after 5 min, which further increased to 90% at 30 min with 98.1 % solketal selectivity. Further increase in reaction time showed a marginal decrease in glycerol conversion (87%) with 98.1% solketal selectivity. A marginal decrease in glycerol conversion after 30 minutes indicates the formation of glycerol by the hydrolysis of ketals due to a reverse reaction. Similar results were obtained for other catalysts also in previous reports [33, 91, 92].

3.2.3. Effect of carbonyl substrates on glycerol reaction

The effect of substrate on catalytic activity was studied using glycerol and carbonyl compounds present in different structural environment like acetone, benzaldehyde and furfuraldehyde in order to understand the variations in product selectivity (Table 4). It is observed that for acetone as a reactant, selectivity to 5-membered ring molecule (98%) was favored, while for furfuraldehyde, more of 5-membered (68%) than 6-membered (32%) acetal was obtained. On the other hand, benzaldehyde favors almost equal formation of 5- and 6-membered acetals. It is well-known in the literature that 5-membered ring is kinetically favored, whereas 6-membered ring is thermodynamically favored product [59]. It is clear from the results that ketalization of glycerol with acetone occurs at a lower temperature favouring kinetically preferred 5-membered ketal. For furfuraldehyde and benzaldehyde reactions which occur at higher temperatures, formation of thermodynamically favoured acetal increases. During the first step, 5-membered ring forms at a higher rate than 6-membered ring. In the second step, equilibrium between the two products is reached with increase in degree of conversion for the 6-membered cyclic acetal depending on the thermodynamic conditions.

3.2.4. Reaction mechanism for acetalization and ketalization reactions:

It is found that syntheses of 5 or 6-membered rings from glycerol and carbonyl compounds are catalyzed by Brønsted/Lewis acid sites. However, it is evident from the literature and this study that Brønsted acidic sites are particularly more active than Lewis sites for this reaction. Based on the results obtained, a plausible mechanism is proposed for meso-SnO_2 catalyzed reaction of glycerol with acetone / benzaldehyde as shown in Scheme 3. In the first step, the carbonyl group in acetone/ benzaldehyde was activated by acid sites of the catalyst. In the second step, –OH group of glycerol attacks carbonyl carbon and forms an intermediate called hemiacetal. This intermediate undergoes cyclization by the attack of lone pair of electrons present on either the adjacent or terminal hydroxyl group on tertiary carbon atom leading to the formation of 5 or 6-membered cyclic acetal with the elimination of water molecule in the last step.

3.2.5. Epoxidation of cyclohexene with hydrogen peroxide

Epoxidation of olefins has been extensively studied because epoxides act as precursors for commodity chemicals such as drug intermediates, agrochemicals and food additives respectively [34,35]. Various homogeneous transition metal complexes and heterogeneous catalysts are known for this reaction [93]. Schuchardt et al reported γ-alumina as an active catalyst for epoxidation reaction, in which they discovered that the presence of Al–OH species with weak to moderate Brønsted acidic sites could be responsible for the reaction because they can easily replaced on alumina surface by hydrogen peroxide because of their high mobility thereby creating Al–OOH (hydroperoxy groups) [94,95]. This phenomenon arises due to the polarizing effect of Al (III) ions that can activate the O–O bond facilitating distal oxygen transfer to the nucleophilic olefin. However, the involvement of strong acid sites in the reaction can lead to the catalytic decomposition of H_2O_2 causing an undesirable decrease in oxidant selectivity. Alumina catalyst, though a good example to study this reaction, is not highly active

for converting cyclohexene (35% conversion). Chandra et al reported silica microspheres containing surface hydroxyl groups as efficient epoxidation catalysts [96]. They also confirmed that tertiary silanols groups act as catalytic active sites for olefin epoxidation reaction by DFT calculations. Recently Dalai et al have investigated the application of sulphated SnO_2 as catalyst for olefin epoxidation reaction [97]. Tin incorporated periodic mesoporous organosilicas (Sn–PMOs) have also been effectively used for olefin epoxidation reaction [98]. Anion-resin supported peroxo phosphotungstic acid has been reported to be an efficient catalyst for the synthesis of cyclohexene oxide with 98.1% selectivity using cyclohexene and hydrogen peroxide (cyclohexene conversion is 92.4%) [99]. Epoxidation of cyclohexene with hydrogen peroxide produces cyclohexeneoxide which may undergo hydrolysis by acidic sites resulting in 1,2-cyclohexanediol as a side product (Scheme 4). It is considered to be one of the reasons for low yield of the epoxide in most of the catalysts. On the other hand, side products namely 2-cyclohexen-1-ol and 2-cyclohexen-1-one, are formed through the cyclohexenyl hydroperoxide radical [100]. Hence, it requires a suitable catalyst which selectively catalyzes the reaction to produce cyclohexeneoxide. There are only few reports on Sn catalyzed olefin epoxidation available in the literature [97,98]. Therefore, mesoporous SnO_2 was explored as catalyst for epoxidation of cyclohexene using hydrogen peroxide, since it possesses Sn metal centre to activate H_2O_2 as well as acid sites for activation of olefin.

3.2.5.1. Catalytic activity studies

Meso SnO_2 catalyst was evaluated for cyclohexene epoxidation using aqueous 50% H_2O_2 as green oxidant and acetonitrile as solvent at 80 °C, and results are summarized in Table 5. Firstly, the epoxidation reaction was carried without using a catalyst. It gave 5% cyclohexene conversion in 10 h with 2-cyclohexen-1-one as a major product with 49% selectivity. Formation of 2-cyclohexen-1-one was due to an auto catalysis by thermal reaction, and therefore it requires a suitable catalyst to produce cyclohexeneoxide. When meso-SnO_2-T-350

was used as a catalyst, it showed significant increase in cyclohexene conversion (77%) with high selectivity towards cyclohexeneoxide (92.5%). Further increasing the recation time to 16 h resulted in increase of cyclohexene conversion (94%) with marginal decrease in cyclohexeneoxide selectivity (89%). Notably, meso-SnO_2-TF-350 catalyst exhibited lower cyclohexene conversion (61%) with 82.5% cyclohexeneoxide selectivity. The remarkable catalytic activity of meso-SnO_2-T-350 is attributed to a unique combination of larger surface area and weak acidic sites.

The calcination of meso-SnO_2-T-*x* at different temperatures affected the cyclohexene conversion and cyclohexeneoxide selectivity (Table 5). Lower calcination of meso-SnO_2-T at 300 °C converted 75% of cylcohexene into product with 92.7% selectivty to cyclohexeneoxide. Meso-SnO_2-T-350 gave similar cyclohexene conversion (77%) with 92.5% cyclohexeneoxide selectivity. However, the conversion of cyclohexene significantly decreased from 77 to 30% with marginal decrease in cyclohexeneoxide selectivity (92.5 to 88%) by increasing the calcination temperature >350 °C. The higher catalytic activity of meso-SnO_2-T-350 compared to other tin oxide catalysts is attributed to greater amount of acidity and smaller particle size of the catalyst. Furthermore, the decrease of acidic sites suppresses the conversion of cyclohexene which indicates that the amount and nature of acidic sites greatly influence the epoxidation of cyclohexene.

3.2.6. Catalyst reusability studies

The most active meso-SnO_2-T-350 catalyst for acetalization, ketalization and epoxidation reactions was investigated for its reusability and the results are presented in Fig. 12a-c. It was performed under optimized reaction conditions for four consecutive cycles (Fresh, R-1, R-2 and R-3). After each run, the catalyst was filtered and washed with methanol to remove the adsorbed reactants on the catalyst surface. The catalyst was dried and calcined at 350 °C for 2 h. For acetalization and ketalization reactions, the catalyst showed good

recyclability with a marginal decrease in glycerol conversion (~3%) with similar selectivity to the respective products compared to the fresh catalyst for both the reactions for four consecutive runs (Fig. 12a,b). In case of epoxidation reaction, the conversion of cyclohexene varied marginally after the first cycle with a slight variation in cyclohexeneoxide selectivity (Fig. 12c). However, the catalyst retained its catalytic activity till fourth cycle with marginal loss in cyclohexene conversion. The structural integrity of the recycled catalyst was investigated by X-ray diffraction as shown in Fig. 12d. The XRD pattern of the spent meso-SnO_2-T-350 catalyst for all the three reactions matched well with the characteristic peaks of fresh catalyst indicating no change in structure of the catalyst even after four consecutive cycles. These results suggest that meso-SnO_2-T-350 catalyst is stable and reusable without any appreciable loss in activity, and therefore it offers good opportunity for potentially wide applications in catalysis.

4. Conclusions

Mesoporous tin oxide catalysts were prepared by two different synthetic approaches *viz.* template assisted and template-free methods and calcination temperature was varied to generate acidic sites of different nature, strength and amounts. The materials were well-characterized by various techniques and catalytic efficiency was evaluated for acetalization and ketalization of glycerol with benzaldehyde and acetone respectively. The chemical shift of meso-SnO_2-T-350 from ^{1}H MAS NMR indicated the presence of relatively stronger acidic sites than that of other meso-SnO_2 catalysts. Catalytic performance of meso-SnO_2 was compared with other well-known conventional solid acid catalysts. Template assisted meso-SnO_2 catalyst exhibited excellent catalytic performance as compared to other catalysts. The superior catalytic performance of mesoporous tin oxide catalyst was mainly attributed to the presence of its mesoporosity and higher B/L ratio. Template-free mesoporous tin oxide gave lower catalytic activity compared to template assisted method due to the presence lower surface area and lower

amount of active sites. Among meso tin oxide catalysts with different calcination temperatures, meso-SnO_2-T-350 gave highest activity which could be mainly attributed to the presence of high amount of active sites. A good correlation of catalytic activity in these reactions with amount of acidic sites and B/L ratio were observed. Meso-SnO_2 catalysts were also evaluated for epoxidation of cyclohexene with hydrogen peroxide. Meso-SnO_2 calcined at 350 °C gave better catalytic performance than other meso tin oxides due to the presence of higher amount total acidic sites. Reuse of meso-SnO_2 catalyst showed a marginal loss in performance and retained its structure after four cycles. Thus, template assisted mesoporous tin oxide catalyst is proven to be an efficient catalyst for acetalization, ketalization and epoxidation reactions.

Acknowledgements

PM acknowledges Admar Mutt Education Foundation (AMEF), Bengaluru for providing a scholarship and thankful to Manipal University for permitting this research as a part of the Ph.D. program. Authors are thankful to CeNSE, Indian Institute of Science, Bengaluru for SEM analysis.

References

[1] A. Corma, Chem. Rev. 97 (1997) 2373-2420.

[2] S. Fujita, S. Inagaki, Chem. Mater. 20 (2008) 891-908.

[3] C. Kresge, M. Leonowicz, W. Roth, J. Vartuli, J. Beck, Nature 359 (1992) 710-712.

[4] R.M. Martín-Aranda, J. Čejka, Top. Catal. 53 (2010) 141-153.

[5] N. Pal, A. Bhaumik, RSC Adv. 5 (2015) 24363-24391.

[6] A. Taguchi, F. Schüth, Micropor. Mesopor. Mater. 77 (2005) 1-45.

[7] D. Gu, F. Schüth, Chem. Soc. Rev. 43 (2014) 313-344.

[8] M.B. Gawande, R.K. Pandey, R.V. Jayaram, Catal. Sci. Technol. 2 (2012) 1113-1125.

[9] M. Moliner, Y. Román-Leshkov, M.E. Davis, Proc. Natl. Acad. Sci. 107 (2010) 6164-6168.

[10] J. Dijkmans, M. Dusselier, D. Gabriëls, K. Houthoofd, P.C. Magusin, S. Huang, Y. Pontikes, M. Trekels, A. Vantomme, L. Giebeler, ACS Catal. 5 (2015) 928-940.

[11] H.J. Cho, P. Dornath, W. Fan, ACS Catal. 4 (2014) 2029-2037.

[12] E. Nikolla, Y. R-Leshkov, M. Moliner, M.E. Davis, ACS Catal. 1 (2011) 408-410.

[13] Q. Guo, F. Fan, E.A. Pidko, W.N. Van der Graaff, Z. Feng, C. Li, E.J. Hensen, ChemSusChem 6 (2013) 1352-1356.

[14] N.K. Mal, A.V. Ramaswamy, J. Mol. Catal. A: Chem. 105 (1996) 149-158.

[15] P.S. Niphadkar, M.S. Kotwal, S.S. Deshpande, V.V. Bokade, P.N. Joshi, Mater. Chem. Phys. 114 (2009) 344-349.

[16] N.K. Mal, A.V. Ramaswamy, Appl. Catal. A: Gen. 143 (1996) 75-85.

[17] E. Alarcón, C.M. de Correa, Chem. Commun. (2002) 2654-2655.

[18] A.L. Villa, L.F. Correa, E.A. Alarcón, Chem. Eng. J. 215 (2013) 500-507.

[19] V.S. Marakatti, G.V. Shanbhag, A.B. Halgeri, RSC Adv. 3 (2013) 10795-10800.

[20] A. Corma, M.T. Navarro, M. Renz, J. Catal. 219 (2003) 242-246.

[21] T. Toupance, H.E. Hamzaoui, B. Jousseaume, H. Riague, I. Saadeddin, G. Campet, J. Brötz, Chem. Mater. 18 (2006) 6364-6372.

[22] V.S. Marakatti, P. Manjunathan, A.B. Halgeri, G.V. Shanbhag, Catal. Sci. Technol. 6 (2016) 2268-2279.

[23] S. Sandesh, P. Manjunathan, A.B. Halgeri, G.V. Shanbhag, RSC Adv. 5 (2015) 104354-104362.

[24] R. Liu, T. Wang, Y. Jin, Catal. Today 233 (2014) 127-132.

[25] P. Manjunathan, M. Kumar, S.R. Churipard, S. Sivasankaran, G.V. Shanbhag, S.P. Maradur, RSC Adv. 6 (2016) 82654-82660.

[26] P. Manjunathan, R. Ravishankar, G.V. Shanbhag, ChemCatChem 8 (2016) 631-639.

[27] S. Sandesh, G.V. Shanbhag, A.B. Halgeri, Catal. Lett. 143 (2013) 1226-1234.

[28] Y. Nakagawa, Y. Shinmi, S. Koso, K. Tomishige. J. Catal. 272 (2010) 191-194.

[29] Z. Zheng, M. Luo, J. Yu, J. Wang, J. Ji, Ind. Eng. Chem. Res. 51 (2012) 3715-3721.

[30] P. Manjunathan, S.P. Maradur, A. Halgeri, G.V. Shanbhag, J. Mol. Catal. A: Chem. 396 (2015) 47-54.

[31] A. Behr, J. Eilting, K. Irawadi, J. Leschinski, F. Lindner, Green Chem. 10 (2008) 13-30.

[32] A.J. Showler, P.A. Darley, Chem. Rev. 67 (1967) 427-440.

[33] S. Sandesh, A. Halgeri, G.V. Shanbhag, J. Mol. Catal. A: Chem. 401 (2015) 73-80.

[34] B.S. Lane, K. Burgess, Chem. Rev. 103 (2003) 2457-2474.

[35] A.K. Yudin, Aziridines and epoxides in organic synthesis, John Wiley & Sons, 2006.

[36] J. Kasai, Y. Nakagawa, S. Uchida, K. Yamaguchi, N. Mizuno, Chem. Eur. J 12 (2006) 4176-4184.

[37] Y. Wang, C. Ma, X. Sun, H. Li, Micropor. Mesopor. Mater. 49 (2001) 171-178.

[38] Y.-D. Wang, C.L. Ma, X.-D. Sun, Inorg. Chem. Commun. 4 (2001) 223-226.

[39] K.N. Tayade, M. Mishra, J. Mol. Catal. A: Chem. 382 (2014) 114-125.

[40] R.V. Grieken, J. Escola, J. Moreno, R. Rodriguez, Chem. Eng. J. 155 (2009) 442-450.

[41] C. Simons, U. Hanefeld, I.W. Arends, R.A. Sheldon, T. Maschmeyer, Chem. Eur. J 10 (2004) 5829-5835.

[42] J. Wang, Y. Su, J. Xu, C. Ye, F. Deng, Phys. Chem. Chem. Phys. 8 (2006) 2378-2384.

[43] K. Severin, T.M. Abdel-Fattah, Chem. Commun. (1998) 1471-1472.
[44] H. Jiang, D. Hongxing, X. Yunsheng, H. Hong, Chin. J. Catal. 31 (2010) 295-301.
[45] H. Che, S. Han, W. Hou, A. Liu, X. Yu, Y. Sun, S. Wang, Micropor. Mesopor. Mater. 130 (2010) 1-6.
[46] P. Sudarsanam, P. Selvakannan, S.K. Soni, S.K. Bhargava, B.M. Reddy, RSC Adv. 4 (2014) 43460-43469.
[47] B. Mallesham, P. Sudarsanam, B.V.S. Reddy, B.M. Reddy, Appl. Catal. B: Environ. 181 (2016) 47-57.
[48] B. Mallesham, P. Sudarsanam, G. Raju, B.M. Reddy, Green Chem. 15 (2013) 478-489.
[49] Y. Wang, T. Yokoi, R. Otomo, J. N. Kondo, T. Tatsumi, Appl. Catal. A: Gen. 490 (2015) 93-100.
[50] Z. Liu, H. Chen, W. Huang, J. Gu, W. Bu, Z. Hua, J. Shi, Micropor. Mesopor. Mater. 89 (2006) 270-275.
[51] W. Dai, C. Wang, B. Tang, G. Wu, N. Guan, Z. Xie, M. Hunger, L. Li, ACS Catal. 6 (2016) 2955-2964.
[52] G. Liu, J.-G. Jiang, B. Yang, X. Fang, H. Xu, H. Peng, L. Xu, Y. Liu, P. Wu, Micropor. .Mesopor. Mater. 165 (2013) 210-218.
[53] Z. Zhang, L. Wang, Y. Jin, F. Xiao, S. Wang, Part. Part. Sys. Charact. 33 (2016) 519-523.
[54] A. Kar, S. Sain, S. Kundu, A. Bhattacharyya, S. Kumar Pradhan, A. Patra, ChemPhysChem 16 (2015) 1017-1025.
[55] K. Wang, M.C. Hawley, S.J. DeAthos, Ind. Eng. Chem. Res. 42 (2003) 2913-2923.
[56] C. -H. Zhou, J. N. Beltramini, Y. -X. Fan, G. Q. Lu, Chem. Soc. Rev. 37 (2008) 527–549.
[57] S.B. Umbarkar, T.V. Kotbagi, A.V. Biradar, R. Pasricha, J. Chanale, M.K. Dongare, A.-S. Mamede, C. Lancelot, E. Payen, J. Mol. Catal. A: Chem. 310 (2009) 150-158.
[58] P. Sudarsanam, B. Mallesham, A.N. Prasad, P.S. Reddy, B.M. Reddy, Fuel Process Technol. 106 (2013) 539-545.
[59] J. Deutsch, A. Martin, H. Lieske, J. Catal. 245 (2007) 428-435.
[60] B. Mallesham, P. Sudarsanam, B.M. Reddy, Ind. Eng. Chem. Res. 53 (2014) 18775-18785.
[61] N. Narkhede, A. Patel, RSC Adv. 4 (2014) 19294-19301.
[62] C. Gonzalez-Arellano, R.A. Arancon, R. Luque, Green Chem. 16 (2014) 4985-4993.
[63] C. Gonzalez-Arellano, S. De, R. Luque, Catal. Sci. Technol. 4 (2014) 4242-4249.
[64] H. Li, D. Gao, P. Gao, F. Wang, N. Zhao, F. Xiao, W. Wei, Y. Sun, Catal. Sci. Technol. 3 (2013) 2801-2809.
[65] J.A. Melero, G. Vicente, G. Morales, M. Paniagua, J. Bustamante, Fuel 89 (2010) 2011-2018.
[66] M.J. Climent, A. Corma, S. Iborra, Green Chem.16 (2014) 516-547.
[67] A. Maksimov, A. Nekhaev, D. Ramazanov, Y.A. Arinicheva, A. Dzyubenko, S. Khadzhiev, Petrol. Chem. 51 (2011) 61-69.
[68] F.D. Menezes, M.D. Guimaraes, M.r.J. da Silva, Ind. Eng. Chem. Res. 52 (2013) 16709-16713.
[69] M.J. da Silva, F. de Ávila Rodrigues, A.A. Júlio, Chem. Eng. J. 307 (2017) 828-835.
[70] M.J. da Silva, A.A. Julio, F.C.S Dorigetto, RSC Adv. 5 (2015) 44499-44506.

[71] P. Ferreira, I. Fonseca, A. Ramos, J. Vital, J. Castanheiro, Appl Catal B: Environ. 98 (2010) 94-99.
[72] P.S. Reddy, P. Sudarsanam, B. Mallesham, G. Raju, B.M. Reddy, J. Ind. Eng Chem. 17 (2011) 377-381.
[73] C.-N. Fan, C.-H. Xu, C.-Q. Liu, Z.-Y. Huang, J.-Y. Liu, Z.-X. Ye, React. Kinet Mech Cat. 107 (2012) 189-202.
[74] D.C. de Carvalho, A.C. Oliveira, O.P. Ferreira, J.M. Filho, S. T.-Cuapa, A.C. Oliveira, Chem. Eng. J. 313 (2017) 1454–1467.
[75] G. Nair, E. Adrijanto, A. Alsalme, I. Kozhevnikov, D. Cooke, D. Brown, N. Shiju, Catal. Sci. Tech. 2 (2012) 1173-1179.
[76] R. Rodrigues, D. Mandelli, N. S. Gonçalves, P. P. Pescarmona, W.A. Carvalho, J. Mol. Catal. A: Chem. 422 (2016) 422, 122-130.
[77] T.E. Souza, I.D. Padula, M.M. Teodoro, P. Chagas, J.M. Resende, P.P. Souza, L.C. Oliveira, Catal. Today 254 (2015) 83-89.
[78] N. Viswanadham, S. Debnath, P. Sreenivasulu, D. Nandan, S.K. Saxena, H. A. Al-Muhtaseb, RSC Adv. 5 (2015) 67380-67383.
[79] Z. Gui, N. Zahrtmann, S. Saravanamurugan, I. Reyero, Z. Qi, M.A. Bañares, A. Riisager, E.J. Garcia-Suarez, ChemistrySelect 1 (2016) 5869-5873.
[80] L. Wang, J. Zhang, S. Yang, Q. Sun, L. Zhu, Q. Wu, H. Zhang, X. Meng, F.-S. Xiao, J. Mater. Chem. A 1 (2013) 9422-9426.
[81] S.R. Churipard, P. Manjunathan, P. Chandra, G.V. Shanbhag, R. Ravishankar, P.V.C. Rao, G.S. Ganesh, A.B. Halgeri, S.P. Maradur, New J. Chem. 41 (2017) 5745-5751.
[82] D. Nandan, P. Sreenivasulu, L.S. Konathala, M. Kumar, N. Viswanadham, Micropor. Mesopor. Mater. 179 (2013) 182-190.
[83] R. Rodrigues, M. Gonçalves, D. Mandelli, P.P. Pescarmona, W.A. Carvalho, Catal. Sci. Technol. 4 (2014) 2293-2301.
[84] C.X. da Silva, V.L. Gonçalves, C.J. Mota, Green Chem. 11 (2009) 38-41.
[85] G. Vicente, J.A. Melero, G. Morales, M. Paniagua, E. Martín, Green Chem. 12 (2010) 899-907.
[86] K.N. Tayade, M. Mishra, K. Munusamy, R.S. Somani, Catal. Sci. Technol. 5 (2015) 2427-2440.
[87] L. Wang, J. Zhang, X. Wang, B. Zhang, W. Ji, X. Meng, J. Li, D.S. Su, X. Bao, F.-S. Xiao, J. Mater. Chem. A 2 (2014) 3725-3729.
[88] L. Li, D. Cani, P.P. Pescarmona, Inorg. Chim. Acta. 431 (2015) 289-296.
[89] S. Gadamsetti, N.P. Rajan, G.S. Rao, K.V. Chary, J. Mol. Catal. A: Chem. 410 (2015) 49-57.
[90] M.N. Timofeeva, V.N. Panchenko, N.A. Khan, Z. Hasan, I.P. Prosvirin, S.V. Tsybulya, S.H. Jhung, Appl.Catal. A: Gen. 529 (2017) 167-174.
[91] L. Li, T. I. Koranyi, B. F. Sels, P. P. Pescarmona, Green Chem. 14 (2012) 1611-1619.
[92] L. P. Ozorio, R. Pianzolli, M. B. S. Mota, C. J. A. Mota. J. Braz. Chem. Soc. 23 (2012) 931-937.
[93] K.A. Jørgensen, Chem. Rev. 89 (1989) 431-458.
[94] R. Rinaldi, F.Y. Fujiwara, W. Hölderich, U. Schuchardt, J. Catal. 244 (2006) 92-101.

[95] D. Mandelli, M.C.A. van Vliet, R. A. Sheldon, U. Schuchardt, Appl. Catal. A: Gen. 219 (2001) 209-213.
[96] P. Chandra, D. S. Doke, S. B. Umbarkar, K. Vanka, A. V. Biradar, RSC Adv. 5 (2015) 21125-21131.
[97] A. K. Somidi, R. V. Sharma, A. K. Dalai, Ind. Eng. Chem. Res. 53 (2014) 18668-18677.
[98] S. Sisodiya, S. Shylesh, A. Singh, Catal. Commun. 12 (2011) 629-633.
[99] C. Peng, X.-H. Lu, X.-T. Ma, Y. Shen, C.-C. Wei, J. He, D. Zhou, Q.-H. Xia, J. Mol. Catal. A: Chem. 423 (2016) 393-399.
[100] Y. Jiang, Y. Zhao, X. Xu, K. Lin, D. Wang, RSC Adv. 6 (2016) 77481-77488.

Figure Caption

Figures and Schemes

Figures:

Fig. 1. XRD patterns at low (a) and wide (b) angle for meso-SnO_2-T-*x*.

Fig. 2. Nitrogen adsorption-desorption isotherm and pore size distribution of meso-SnO_2-T-*x*.

Fig .3. NH_3-TPD profile of meso-SnO_2 catalysts

Fig. 4. UV-visible DRS spectra of meso SnO_2 catalysts

Fig. 5. ^{1}H MAS NMR (a and b) and ^{119}Sn MAS NMR(c) of meso-SnO_2 catalysts

Fig. 6. SEM images of meso-SnO_2 catalysts and average particle sizes

Fig. 7. TEM image of meso-SnO_2-T-350 (a and b); HRTEM image (c) and insert is FFT pattern; and SAED images (d).

Fig. 8. Correlation plot for glycerol conversion vs total amount of acidity (mmol $NH_{3\ des}$/g) on glycerol acetalization with benzaldehyde. **Reaction conditions:** glycerol = 10 mmol (0.92g), benzaldehyde = 10 mmol (1.06g), catalyst amount = 0.10 g, temp = 100 °C, time = 30 min, N_2 atmosphere.

Fig. 9. Influence of reaction conditions on glycerol conversion and HPD selectivity over meso-SnO_2-T-350 catalyst. **(a) Effect of reaction temperature.** Conditions: glycerol = 10 mmol (0.92 g), benzaldehyde = 10 mmol (1.06 g), catalyst amount = 0.10 g, time = 30 min, N_2 atmosphere. **(b) Effect of reactant mole ratio.** Conditions: catalyst amount = 10 wt% (referred to glycerol weight), temp = 100 °C, time = 30 min, N_2 atmosphere. **(c) Effect of catalyst amount.** Conditions: glycerol = 10 mmol (0.92 g), benzaldehyde = 20 mmol (2.12 g), temp = 100 °C, time = 30 min, N_2 atmosphere, catalyst amount = referred to glycerol weight. **(d) Effect of reaction time.** Conditions: glycerol = 10 mmol (0.92 g), benzaldehyde = 20 mmol (2.12 g), catalyst amount = 0.10 g, temp = 100 °C, N_2 atmosphere.

Fig. 10. Correlation plot for glycerol conversion vs total amount of acidity (mmol $NH_{3\ des}$/g) on glycerol ketalization with acetone. **Reaction conditions:** glycerol = 27 mmol (2.5 g), acetone = 27 mmol (1.6 g), catalyst amount = 0.125 g, temp = 60 °C, time = 30 min.

Fig. 11. Influence of reaction conditions on glycerol conversion and solketal selectivity over meso-SnO_2-T-350 catalyst. **(a) Effect of reaction temperature.** Conditions: glycerol = 27 mmol (2.5 g), acetone = 27 mmol (1.6 g), catalyst amount = 0.125 g, time = 30 min. **(b) Effect of reactant mole ratio.** Conditions: catalyst amount = 5wt% (referred to glycerol weight), temp = 60 °C, time = 30 min. **(c) Effect of catalyst amount.** Conditions: glycerol = 27 mmol (2.5 g), acetone = 135 mmol (7.9 g), temp = 60 °C, time = 30 min, catalyst amount = referred to glycerol weight. **(d) Effect of reaction time.** Conditions: glycerol = 27 mmol (2.5 g), acetone = 135 mmol (7.9 g), catalyst amount = 0.125 g, temp = 60 °C.

Fig. 12. Catalyst reusability studies and study on spent catalyst. **(a) Conditions:** glycerol = 20 mmol (1.84 g), benzaldehyde = 40 mmol (4.24 g), catalyst amount = 0.20 g, temp = 100 °C, time = 30 min, N_2 atmosphere. **(b) Conditions:** glycerol = 54 mmol (5 g), acetone = 270 mmol (15.8 g), catalyst amount = 0.25 g, time = 30 min. **(c) Conditions:** cyclohexene = 20 mmol (1.64 g), 50% H_2O_2 = 80 mmol (5.52 g), acetonitrile (solvent) = 16 ml, catalyst = 0.16 g, temp

= 80 °C, time = 16 h. **(d) XRD patterns of fresh and used catalysts:** R-3-a = after 3 times reused catalyst from acetalization of glycerol with benzaldehyde, R-3-b = after 3 times reused catalyst from ketalization of glycerol with acetone, R-3-c = after 3 times reused catalyst from epoxidation of cyclohexene reaction.

Schemes:

Scheme 1. Reaction scheme for glycerol acetalization with benzaldehyde

Scheme 2. Reaction scheme for glycerol ketalization with acetone

Scheme 3. Plausible mechanistic pathway of acetalization and ketalization of glycerol

Scheme 4. Reaction scheme for cyclohexene epoxidation

Figures

Fig. 1. XRD patterns at low (a) and wide (b) angle for meso-SnO_2-T-*x*.

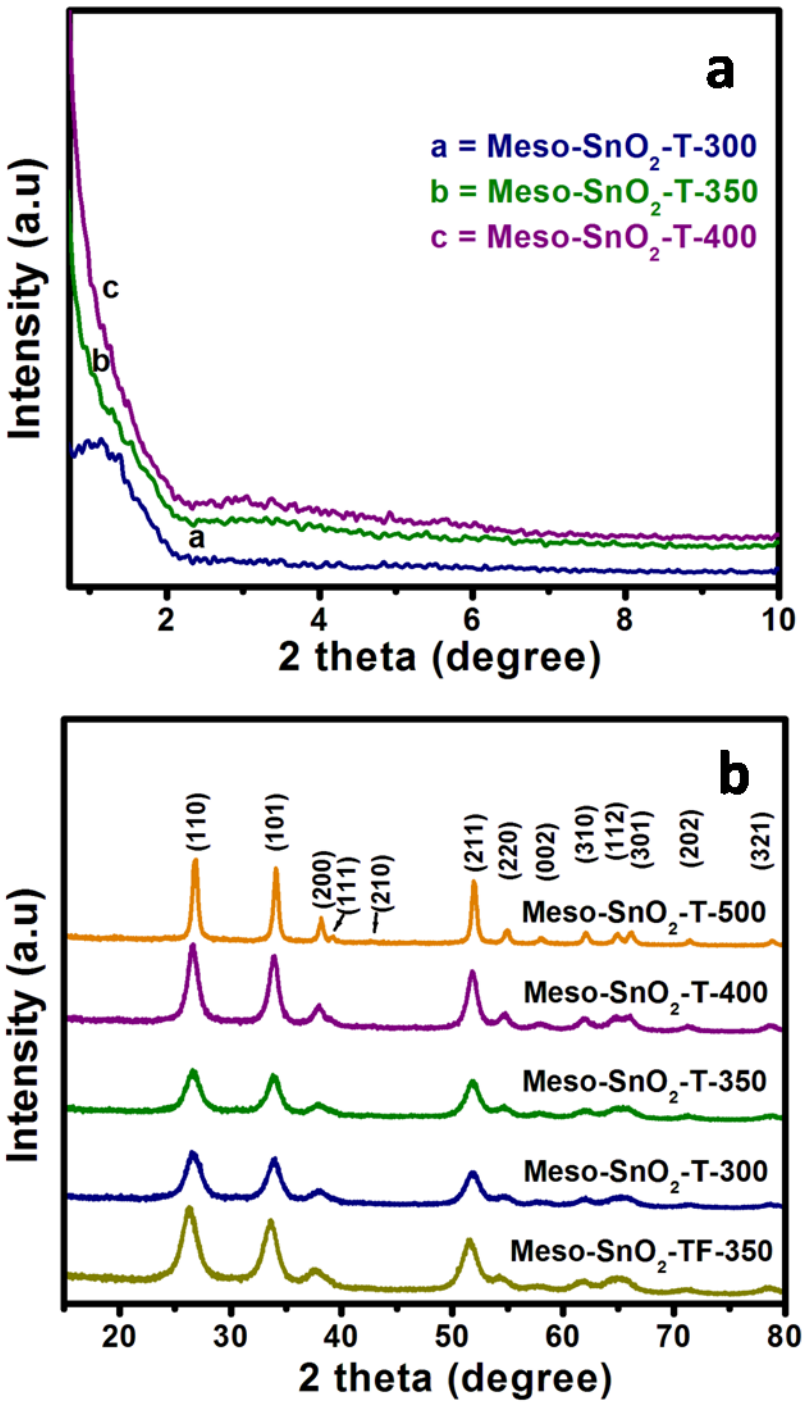

Fig. 2. Nitrogen adsorption-desorption isotherm and pore size distribution of meso-SnO_2-T-*x*.

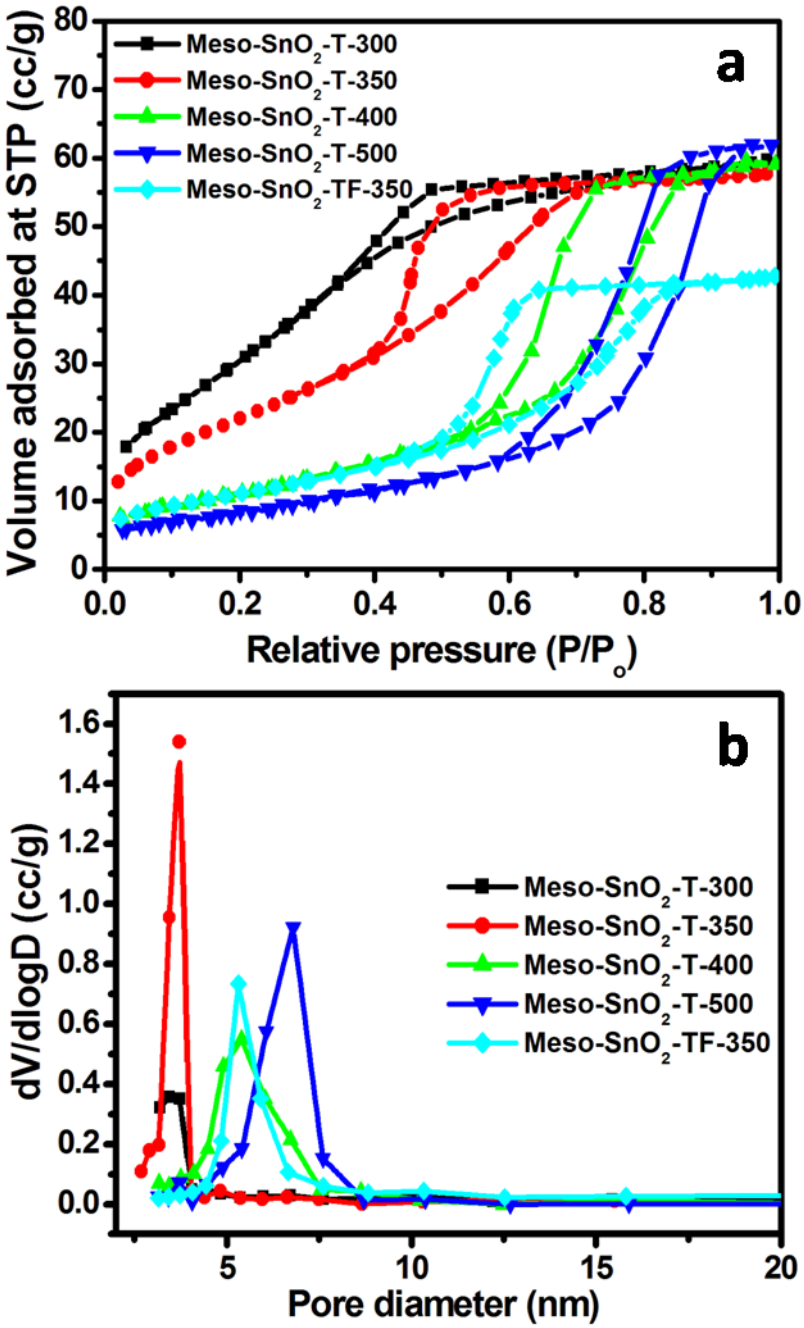

Fig. 3. NH_3-TPD profile of meso-SnO_2 catalysts

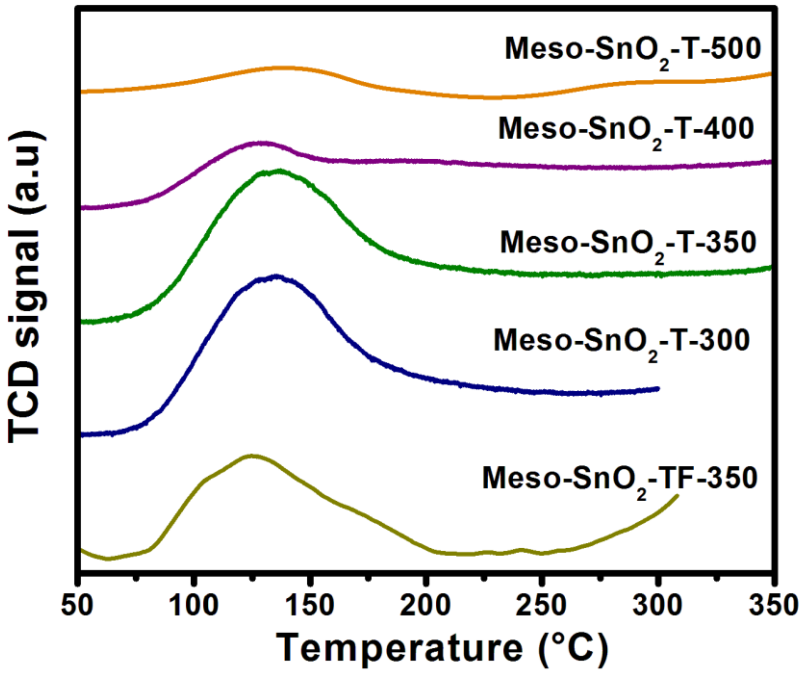

Fig. 4. UV-visible DRS spectra of meso SnO_2 catalysts

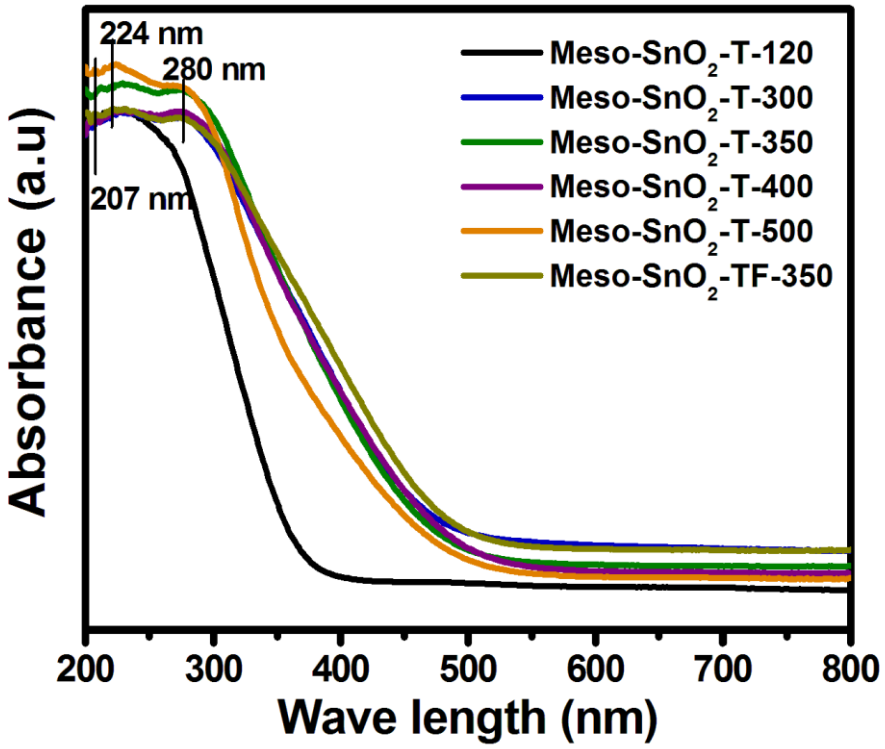

Fig. 5. ^{1}H MAS NMR (a and b) and ^{119}Sn MAS NMR (c) of meso-SnO_2 catalysts

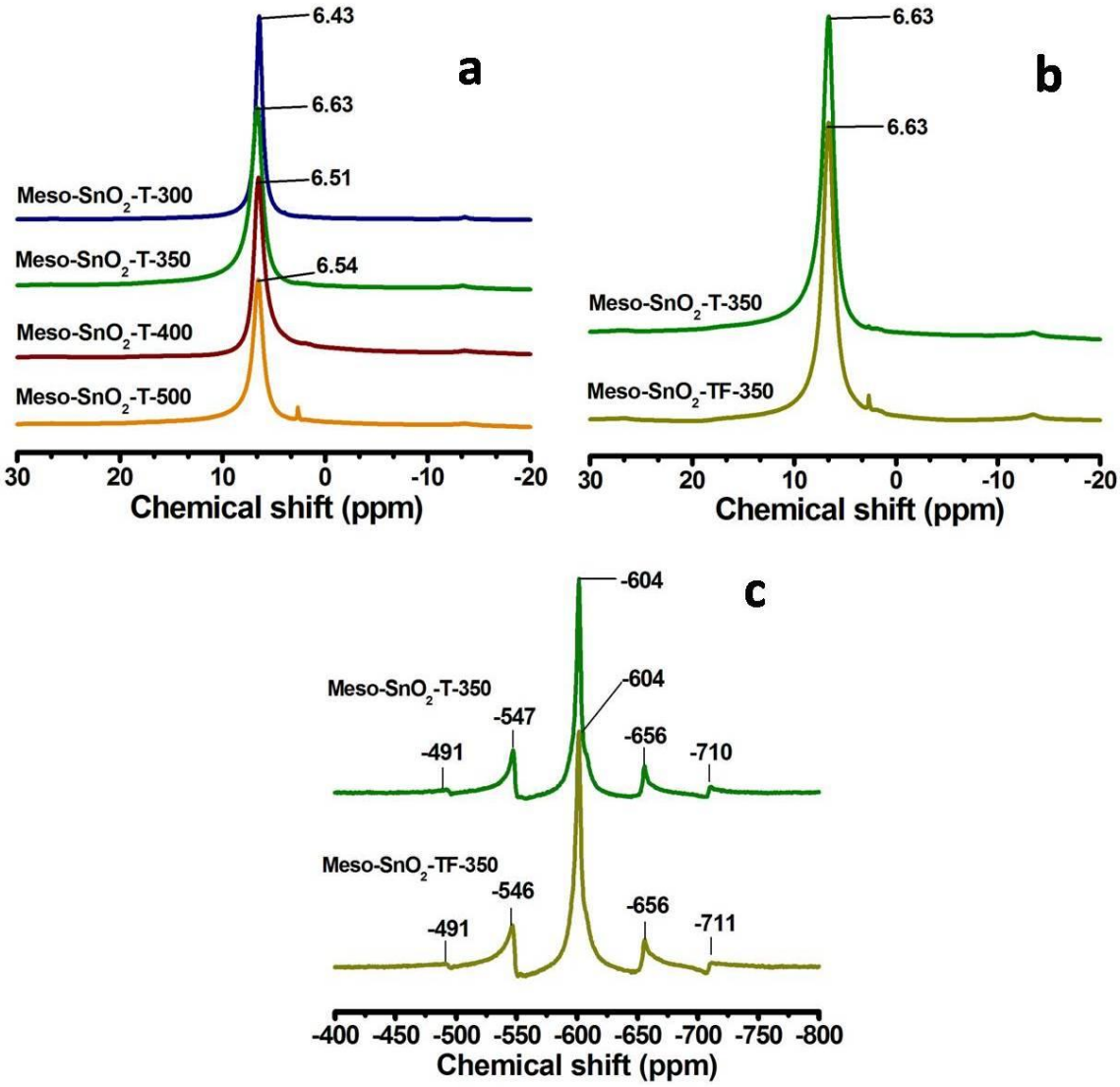

Fig. 6. SEM images of meso-SnO_2 catalysts and average particle sizes

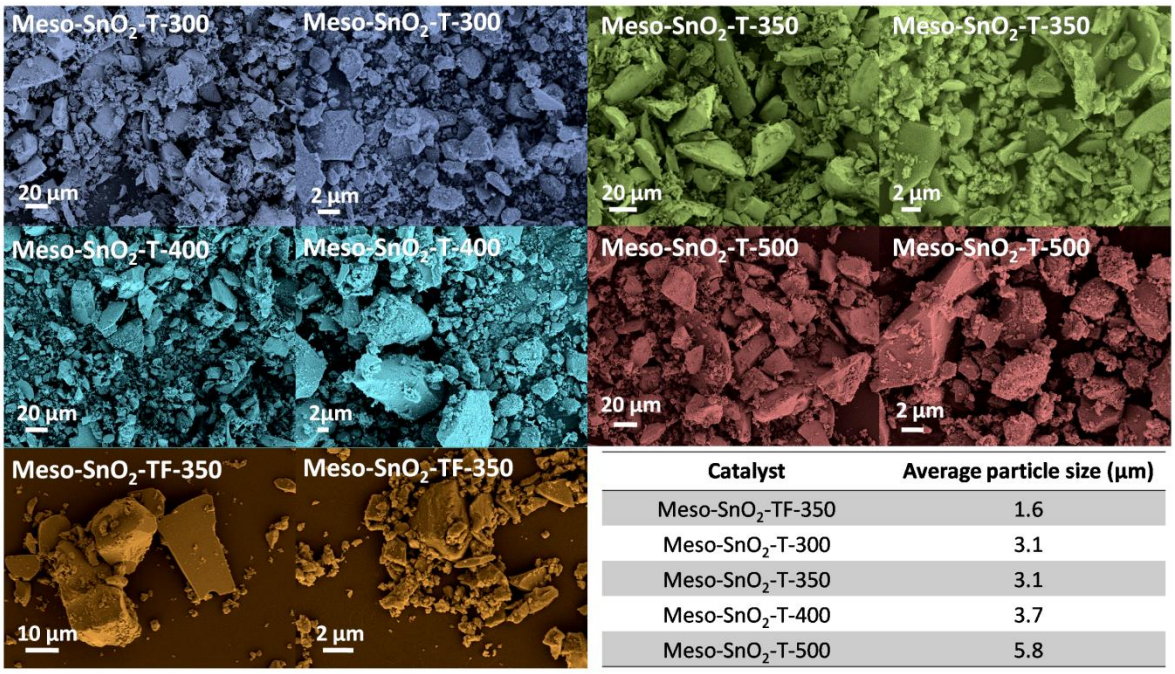

Catalyst	Average particle size (µm)
Meso-SnO_2-TF-350	1.6
Meso-SnO_2-T-300	3.1
Meso-SnO_2-T-350	3.1
Meso-SnO_2-T-400	3.7
Meso-SnO_2-T-500	5.8

Fig. 7. TEM image of meso-SnO_2-T-350 (a and b); HRTEM image (c) and insert is FFT pattern; and SAED images (d).

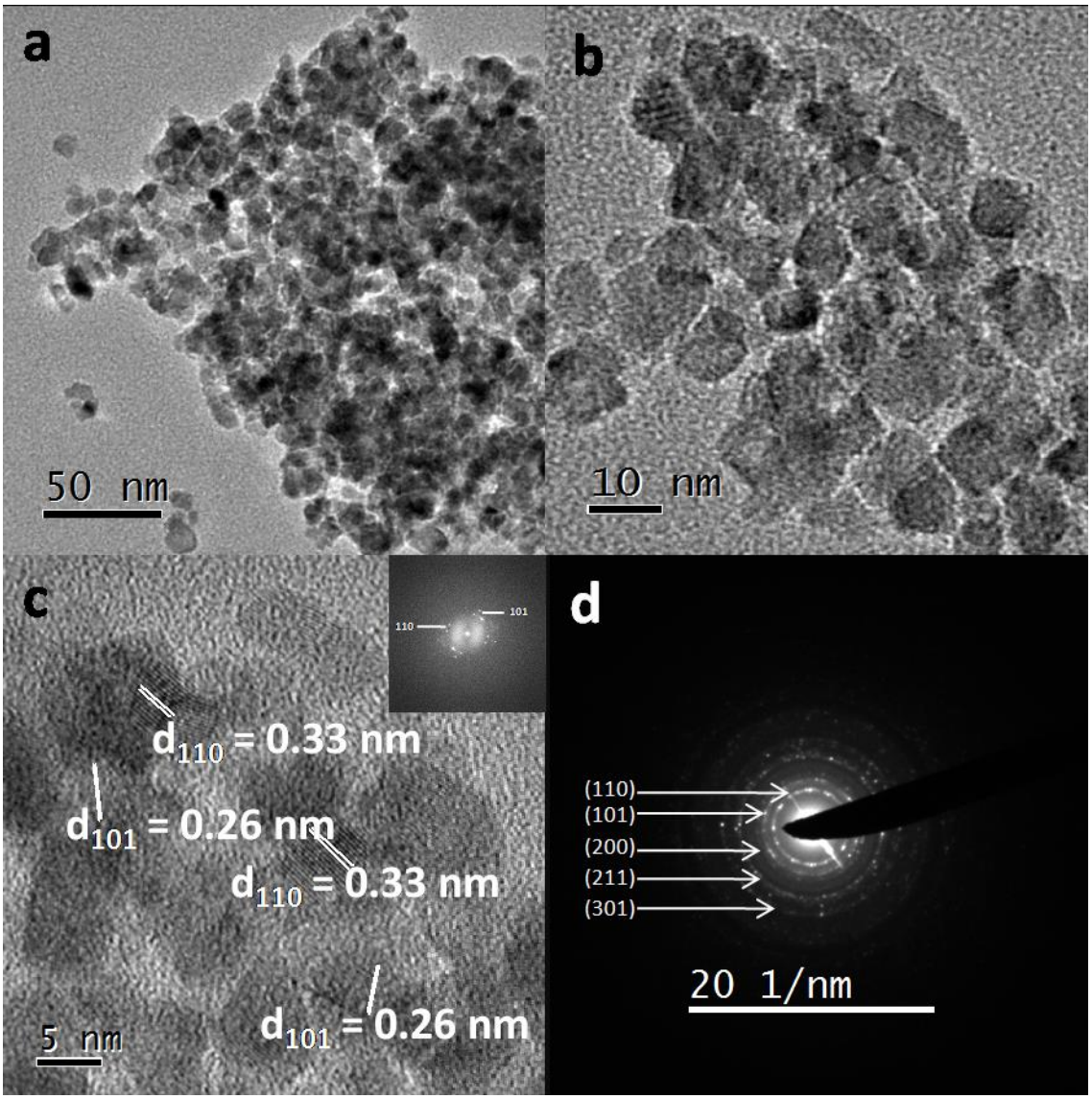

Fig. 8. Correlation plot for glycerol conversion vs total amount of acidity (mmol $NH_{3\ des}$/g) on glycerol acetalization with benzaldehyde.

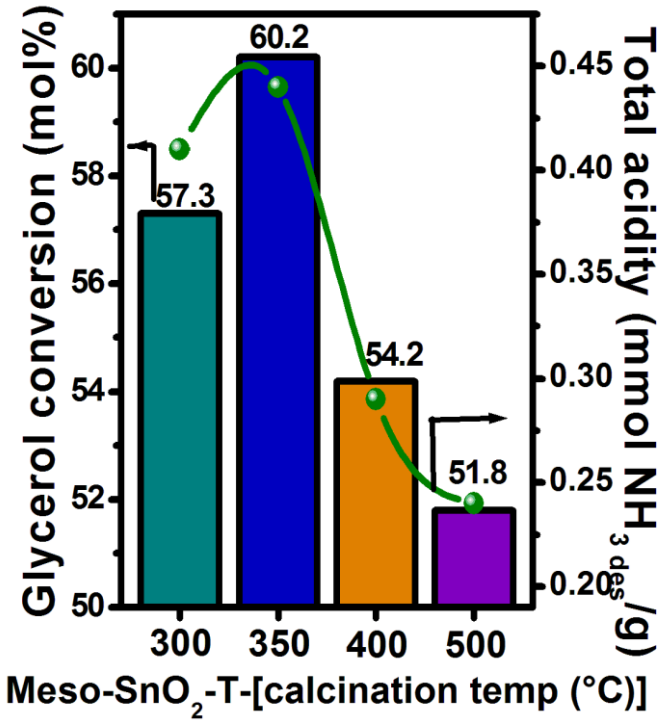

Reaction conditions: glycerol = 10 mmol (0.92 g), benzaldehyde = 10 mmol (1.06 g), catalyst amount = 0.10 g, temp = 100 °C, time = 30 min, N_2 atmosphere.

Fig. 9. Influence of reaction conditions

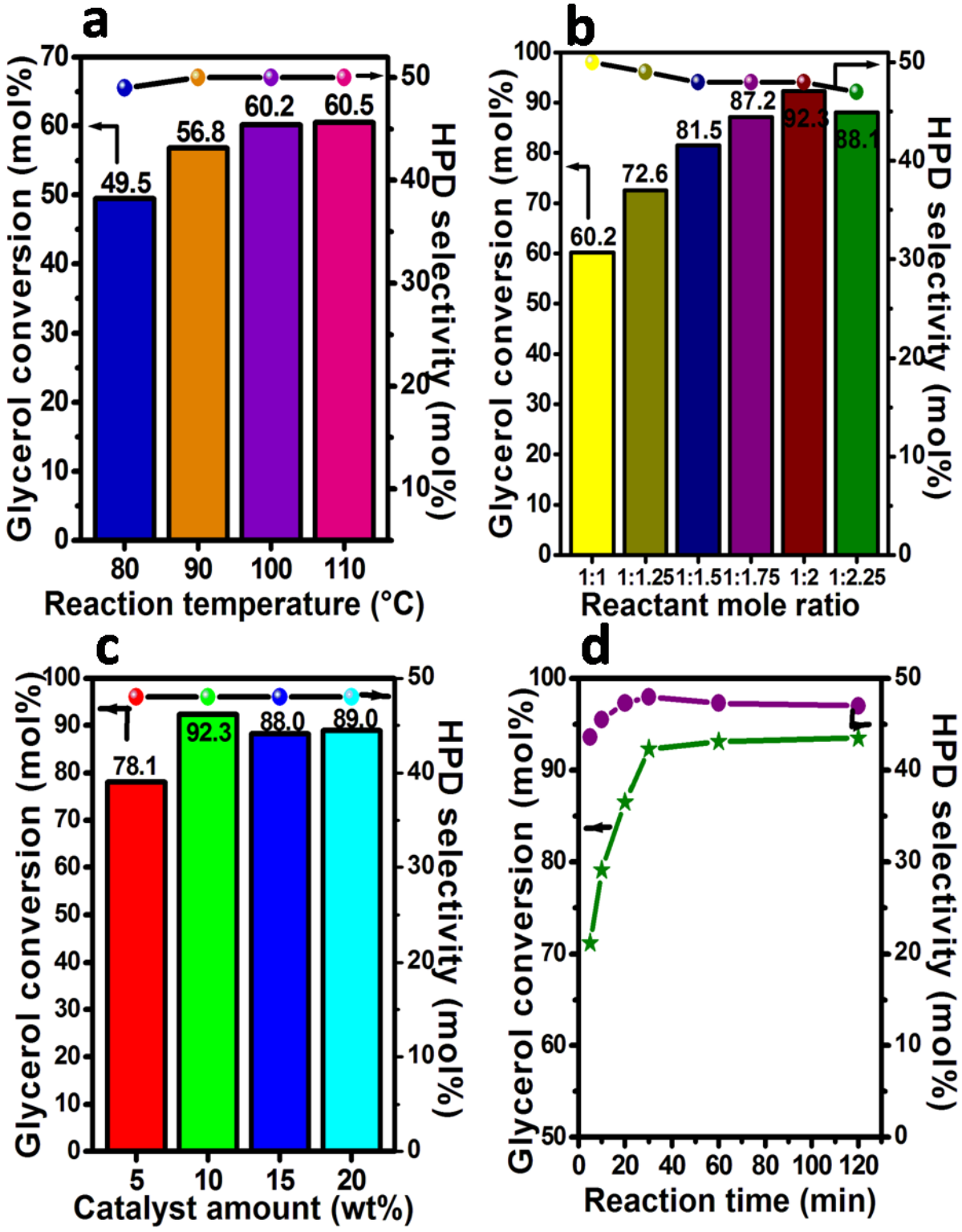

Fig. 9. Influence of reaction conditions on glycerol conversion and HPD selectivity over meso-SnO_2-T-350 catalyst. **(a) Effect of reaction temperature.** Conditions: glycerol = 10 mmol (0.92 g), benzaldehyde = 10 mmol (1.06 g), catalyst amount = 0.10 g, time = 30 min, N_2 atmosphere. **(b) Effect of reactant mole ratio.** Conditions: catalyst amount = 10 wt% (referred

to glycerol weight), temp = 100 °C, time = 30 min, N_2 atmosphere. **(c) Effect of catalyst amount.** Conditions: glycerol = 10 mmol (0.92 g), benzaldehyde = 20 mmol (2.12 g), temp = 100 °C, time = 30 min, N_2 atmosphere, catalyst amount = referred to glycerol weight. **(d) Effect of reaction time.** Conditions: glycerol = 10 mmol (0.92 g), benzaldehyde = 20 mmol (2.12 g), catalyst amount = 0.10 g, temp = 100 °C, N_2 atmosphere.

Fig. 10. Correlation plot for glycerol conversion vs total amount of acidity (mmol $NH_{3\ des}$/g) on glycerol ketalization with acetone.

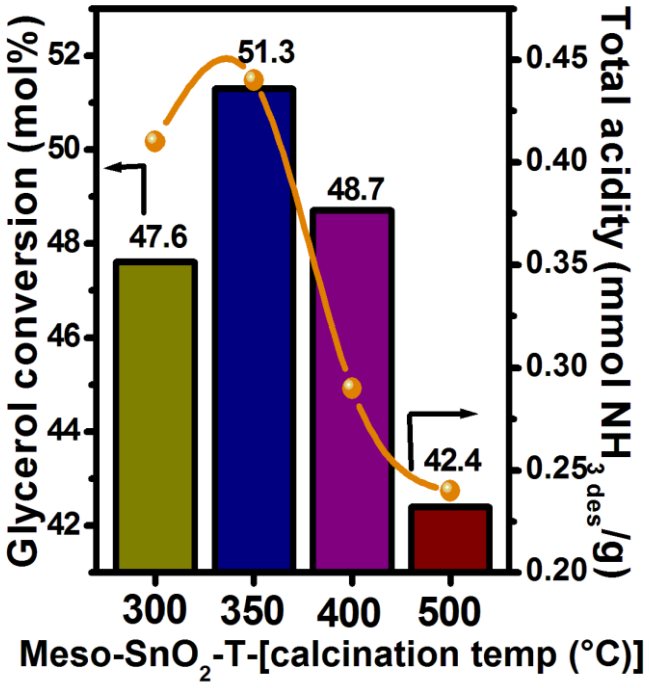

Reaction conditions: glycerol = 27 mmol (2.5 g), acetone = 27 mmol (1.6 g), catalyst amount = 0.125 g, temp = 60 °C, time = 30 min.

Fig. 11. Influence of reaction conditions

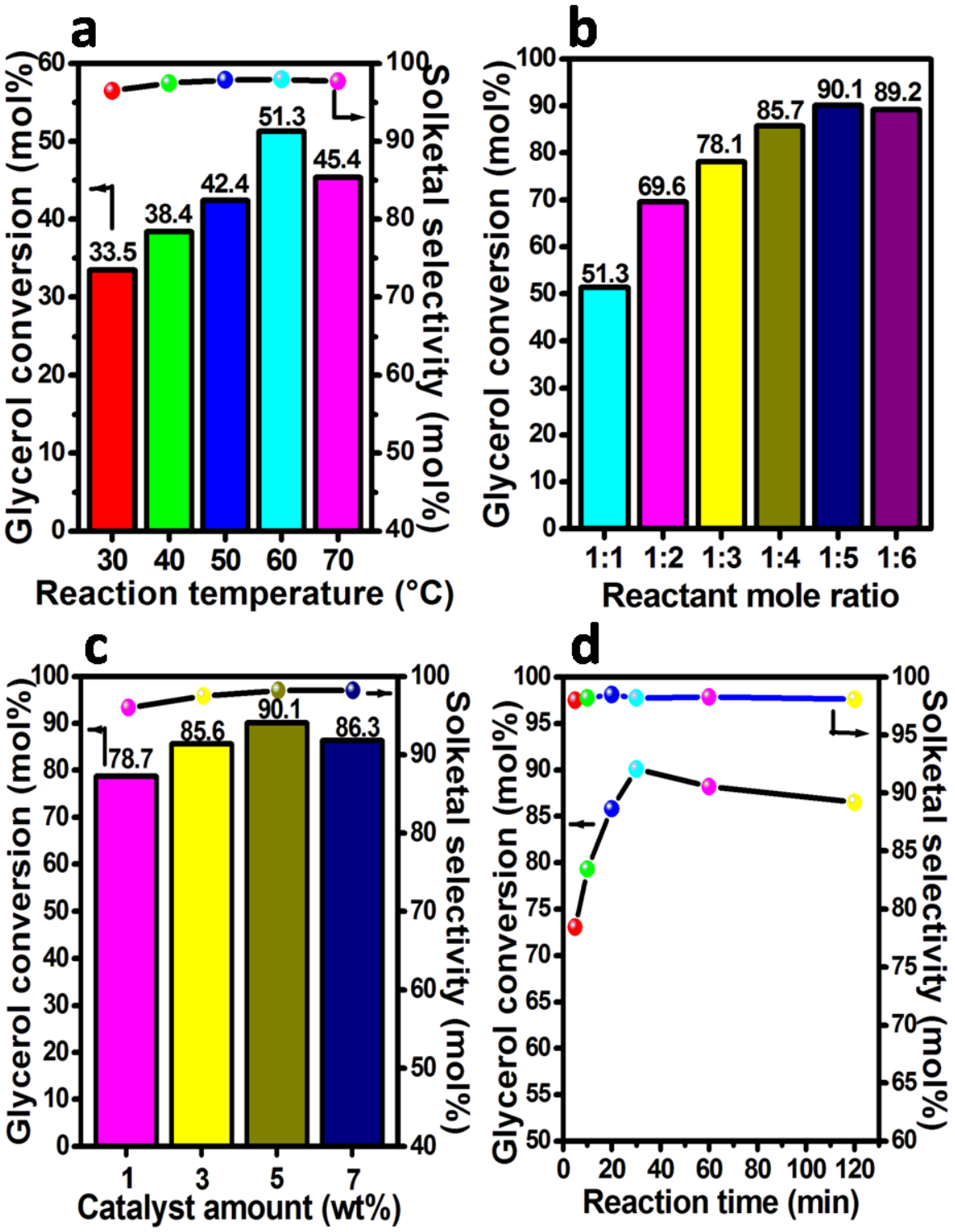

Fig. 11. Influence of reaction conditions on glycerol conversion and solketal selectivity over meso-SnO_2-T-350 catalyst. **(a) Effect of reaction temperature.** Conditions: glycerol = 27 mmol (2.5 g), acetone = 27 mmol (1.6 g), catalyst amount = 0.125 g, time = 30 min. **(b) Effect of reactant mole ratio.** Conditions: catalyst amount = 5wt% (referred to glycerol weight), temp = 60 °C, time = 30 min. **(c) Effect of catalyst amount.** Conditions: glycerol = 27 mmol (2.5 g), acetone = 135 mmol (7.9 g), temp = 60 °C, time = 30 min, catalyst amount = referred

to glycerol weight. **(d) Effect of reaction time.** Conditions: glycerol = 27 mmol (2.5 g), acetone = 135 mmol (7.9 g), catalyst amount = 0.125 g, temp = 60 °C.

Fig. 12. Catalyst reusability studies and study on spent catalyst

Fig. 12. Catalyst reusability studies and study on spent catalyst. **(a) Conditions:** glycerol = 20

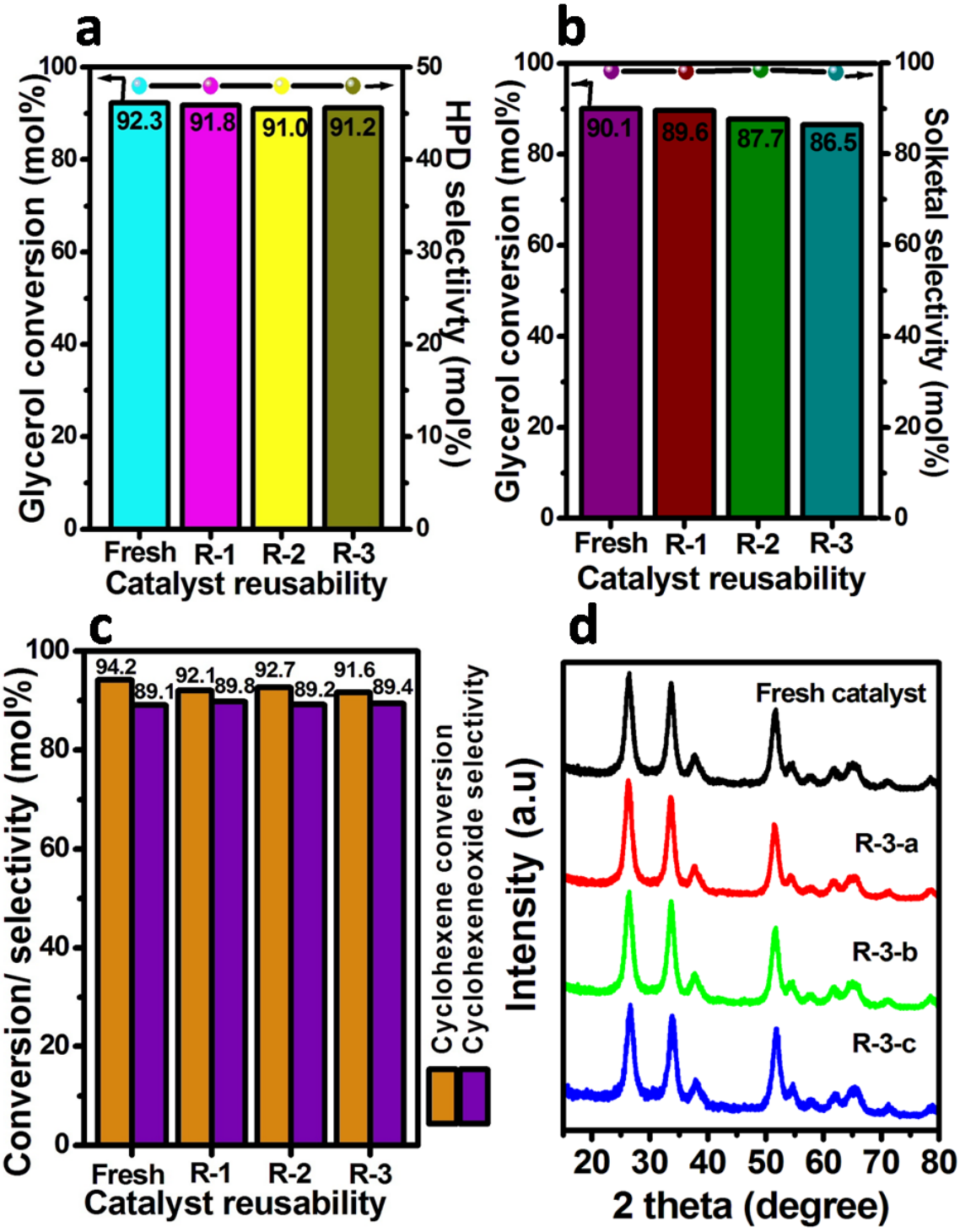

mmol (1.84 g), benzaldehyde = 40 mmol (4.24 g), catalyst amount = 0.20 g, temp = 100 °C, time = 30 min, N_2 atmosphere. **(b) Conditions:** glycerol = 54 mmol (5 g), acetone = 270 mmol (15.8 g), catalyst amount = 0.25 g, time = 30 min. **(c) Conditions:** cyclohexene = 20 mmol (1.64 g), 50% H_2O_2 = 80 mmol (5.52 g), acetonitrile (solvent) = 16 ml, catalyst = 0.16 g, temp = 80 °C, time = 16 h. **(d) XRD patterns of fresh and used catalysts:** R-3-a = after 3 times reused catalyst from acetalization of glycerol with benzaldehyde, R-3-b = after 3 times reused

catalyst from ketalization of glycerol with acetone, R-3-c = after 3 times reused catalyst from epoxidation of cyclohexene reaction.

Scheme 1. Reaction scheme for glycerol acetalization with benzaldehyde

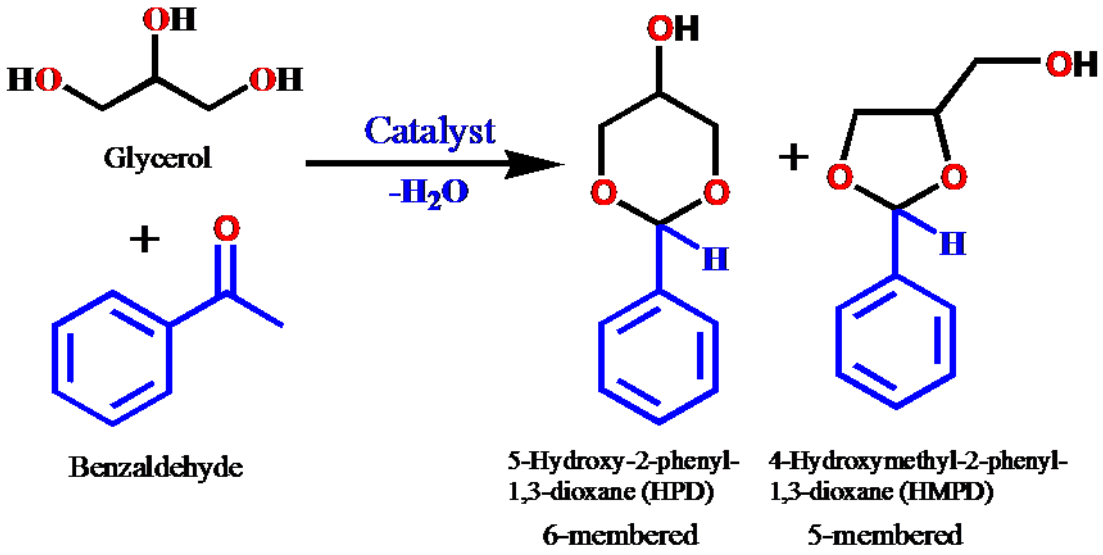

Scheme 2. Reaction scheme for glycerol ketalization with acetone

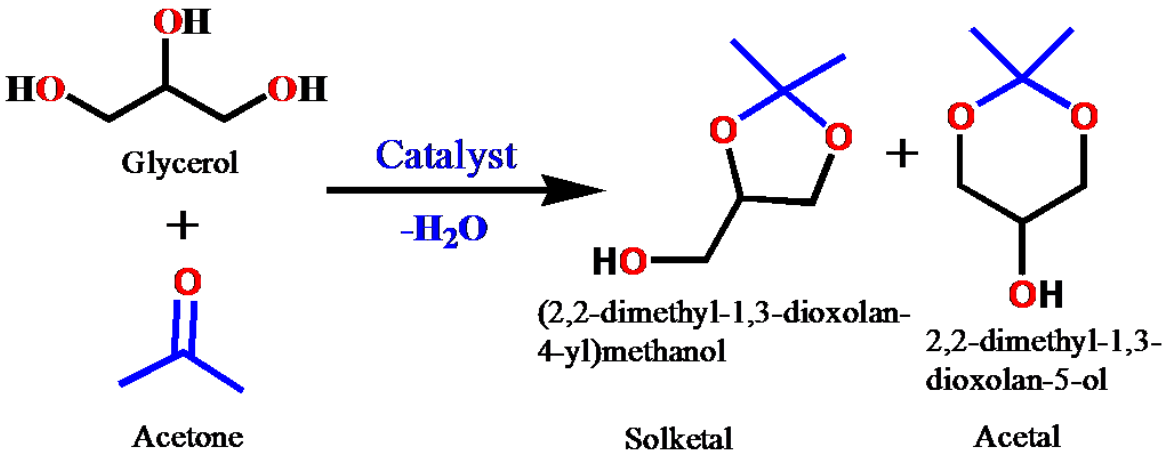

Scheme 3. Plausible mechanistic pathway of acetalization and ketalization reaction of glycerol

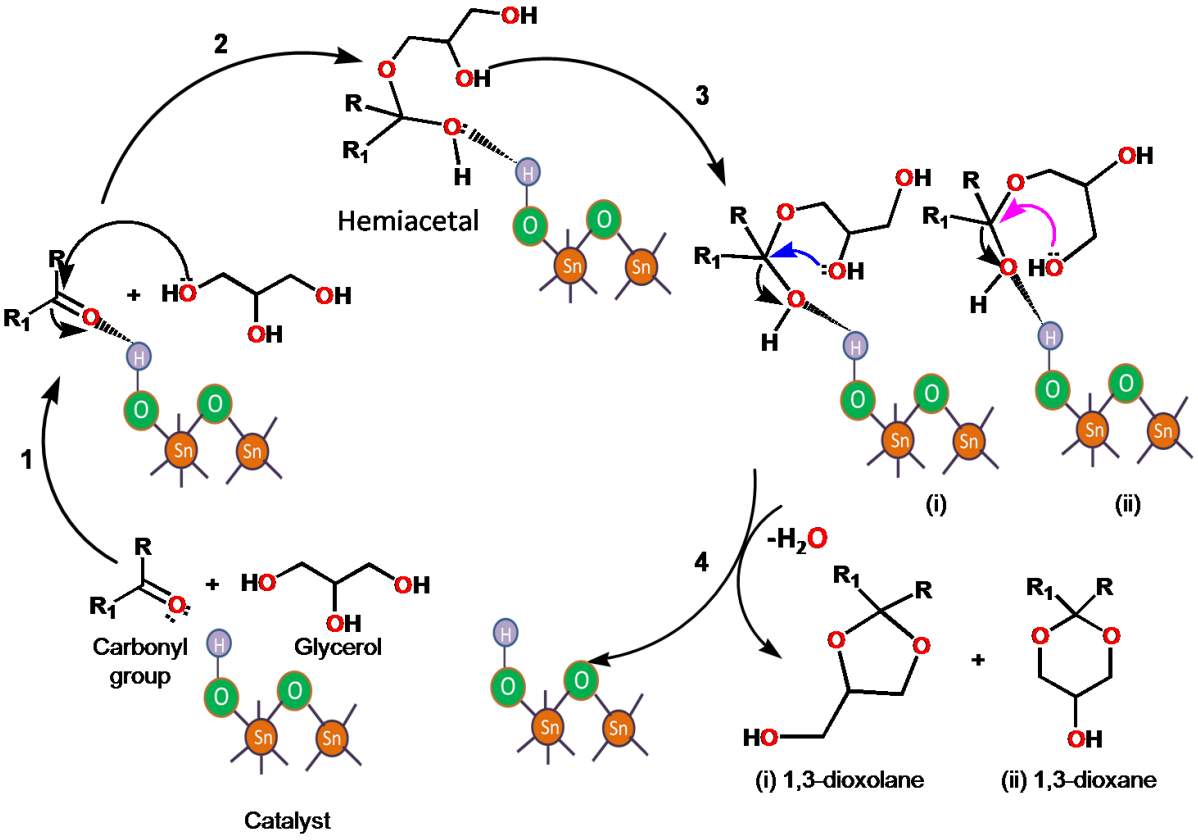

When benzaldehyde as a reactant, R = H, R_1 =C_6H_5.

When acetone as a reactant, R and R_1 = CH_3.

Scheme 4. Reaction scheme for cyclohexene epoxidation

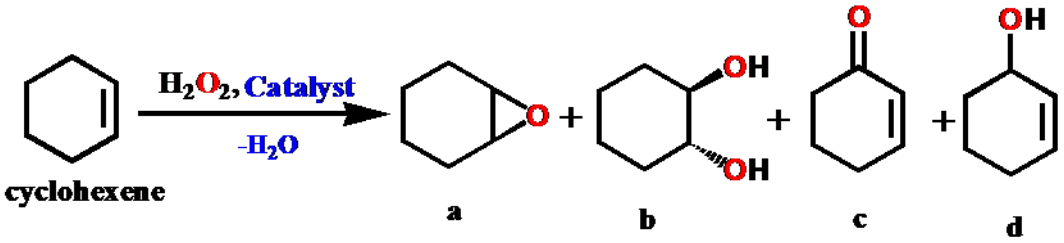

a = Cyclohexeneoxide, b = 1,2-cyclohexanediol, c = 2-cyclohexen-1-one, d = 2-cyclohexen-1-ol

Tables

Table 1. Physico-chemical properties of mesoporous tin oxide and other solid acid catalysts

Catalyst	Calcination temperature (°C)	S_{BET} [a] (m^2/g)	Pore volume [b] (cm^3/g)	Pore size [c] (nm)	B/L ratio[d]	Acidity (mmol NH_3 $_{des}$/g)[e]
Meso-SnO_2-T-300	300	160	0.121	3.4	3.5	0.41
Meso-SnO_2-T-350	350	105	0.110	3.8	3.2	0.44
Meso-SnO_2-T-400	400	55	0.103	5.4	2.5	0.29
Meso-SnO_2-T-500	500	51	0.099	6.8	1.4	0.24
Meso-SnO_2-TF-350	350	50	0.061	5.3	3.0	0.30
Al-MCM-41	500	947	0.758	3.5	1.7	0.76
Al-SBA-15	500	626	1.35	6.2	0.8	0.80
Al-TUD-1	500	600	1.10	15.0	1.9	0.98
H-ZSM-5	540	400	0.30	-	2.3	1.31
H-Mordenite	540	420	0.22	-	1.4	1.84
H-Beta	540	485	0.44	-	1.4	1.51

[a] BET surface area, [b] Total pore volume, [c] Pore diameter, [d] Py-FTIR, [e] NH_3-TPD

Table 2. Catalytic activities of different catalysts for acetalization of glycerol with benzaldehyde reaction[a]

Catalyst	B/L	Acidity (mmol NH_{3des}/g)	Glycerol conv. (mol%)	HPD selec. (mol%)	HPD yield (mol%)	TOF (h^{-1})
Blank	-	-	21.6	46	9.9	-
Meso-SnO_2-T-350	3.2	0.44	60.2	50	30.1	274
Meso-SnO_2-TF-350	3.0	0.30	36.2	47	17.0	241
Al-MCM-41	1.7	1.00	49.9	48	24.0	100
Al-SBA-15	0.8	0.80	47.8	47	22.5	120
Al-TUD-1	1.9	0.98	41.5	48	19.9	85
H-ZSM-5	2.3	1.31	31.7	46	14.6	48
H-Mordenite	1.4	1.84	30.6	47	14.4	33
H-Beta	1.4	1.51	60.4	48	29.0	80
H-Beta[b]	1.4	1.51	42.1	47	19.8	191

Reaction conditions: [a] glycerol = 10 mmol (0.92 g), benzaldehyde = 10 mmol (1.06 g), catalyst amount = 0.10 g, temp = 100 °C, time = 30 min, N_2 atmosphere. [b] 0.044 mmol of acidic sites taken.
TOF (Turn over frequency) = moles of glycerol converted per mole of acidic sites per hour.

Table 3. Catalytic activities of different catalysts for acetalization of glycerol with acetone reaction[a]

Catalyst	B/L	Acidity (mmol NH_{3des}/g)	Glycerol conv. (mol%)	Solketals elec. (mol%)	Solketal yield (mol%)	TOF (h^{-1})
Blank	-	-	0.1	90.0	0.1	-
Meso-SnO_2-T-350	3.2	0.44	51.3	98.0	50.3	506
Meso-SnO_2-TF-350	3.0	0.30	29.0	96.0	27.8	420
Al-MCM-41	1.7	1.00	35.5	94.2	33.4	154
Al-SBA-15	0.8	0.80	26.1	96.3	25.1	142
Al-TUD-1	1.9	0.98	10.2	89.0	9.1	45
H-ZSM-5	2.3	1.31	34.1	94.0	32.1	113
H-Mordenite	1.4	1.84	10.2	89.5	9.1	24
H-Beta	1.4	1.51	47.4	98.5	46.7	136
H-Beta[b]	1.4	1.51	38.8	97.6	37.9	383

Reaction conditions: [a] glycerol (27 mmol = 2.5 g), acetone (27 mmol = 1.6 g), catalyst amount = 0.125 g, temp = 60 °C, time = 30 min. [b] = 0.055 mmol of acidic sites was taken. TOF (Turn over frequency) = moles of glycerol converted per mole of acidic sites per hour.

Table 4. Effect of carbonyl substrates on glycerol reaction

Substrate	Glycerol Conv. (mol%)	Selectivity (%)	
		5-membered	6-membered
Acetone[a]	51.3	98	2
Furfuraldehyde[b]	49.8	68	32
Benzaldehyde[b]	52.5	50	50

Reaction condions: glycerol (10 mmol), substrate (10 mmol), catalyst (meso-SnO_2-T-350) = 0.05 g, time = 30 min, [a] temp = 60 °C, [b] temp = 100 °C.

Table 5. Catalytic activities of meso SnO_2 catalysts for epoxidation of cyclohexene with hydrogen peroxide

Catalyst	B/L	Acidity (mmol NH_{3des}/g)	Time (h)	Cyclohexene conv. (mol%)	Selectivity (mol %)			
					a	b	c	d
Blank	-	-	10	5.0	24.0	-	49.0	27.0
Meso-SnO_2-TF-350	3.0	0.30	10	61.3	86.1	2.3	11.6	-
Meso-SnO_2-T-300	3.5	0.41	10	75.0	92.7	2.9	4.4	-
Meso-SnO_2-T-350	3.2	0.44	10	77.1	92.5	3.2	4.3	-
Meso-SnO_2-T-350	3.2	0.44	12	83.3	91.1	4.0	4.9	-
Meso-SnO_2-T-350	3.2	0.44	16	94.2	89.1	5.1	5.8	-
Meso-SnO_2-T-400	2.5	0.28	10	66.7	91.8	3.3	4.9	-
Meso-SnO_2-T-500	1.4	0.24	10	30.5	88.0	1.5	10.5	-

Reaction conditions: cyclohexene = 10 mmol (0.82 g), 50% H_2O_2 = 40 mmol (2.76 g), acetonitrile (solvent) = 8 ml, catalyst = 0.08 g, temp= 80 °C. a = cyclohexeneoxide, b = 1,2-cyclohexanediol, c = 2-cyclohexen-1-one, d = 2-cyclohexen-1-ol